General Disclaimer

One or more of the Following Statements may affect this Document

- This document has been reproduced from the best copy furnished by the organizational source. It is being released in the interest of making available as much information as possible.

- This document may contain data, which exceeds the sheet parameters. It was furnished in this condition by the organizational source and is the best copy available.

- This document may contain tone-on-tone or color graphs, charts and/or pictures, which have been reproduced in black and white.

- This document is paginated as submitted by the original source.

- Portions of this document are not fully legible due to the historical nature of some of the material. However, it is the best reproduction available from the original submission.

SPACE ASTRONOMY

OF THE

STEWARD OBSERVATORY

THE UNIVERSITY OF ARIZONA
TUCSON, ARIZONA

FINAL TECHNICAL REPORT

OF

NATIONAL AERONAUTICS AND SPACE ADMINISTRATION

GRANT NSG - 7142

June 1976

A 76-11

FINAL TECHNICAL REPORT

OF

NATIONAL AERONAUTICS AND SPACE ADMINISTRATION

Grant NSG-7142

"Evaluation of a Large Format Image Tube Camera for the Shuttle Sortie Mission"

W. C. Tifft
Principal Investigator

Eric R. Craine
Research Associate

Steward Observatory
University of Arizona
Tucson, Arizona

June 1976

A76-11

TABLE OF CONTENTS

I. INTRODUCTION

This report deals with the evaluation of a large format image tube camera of a type under consideration for use on the Space Shuttle Sortie Missions. Our evaluation covers the following subjects

1. resolving power of the system
2. geometrical characteristics of the system (distortion etc.)
3. shear characteristics of the fiber optic coupling
4. background effects in the tube
5. uniformity of response of the tube (as a function of wavelength)
6. detective quantum efficiency (DQE) of the system
7. astronomical applications of the system

It must be noted that many of these characteristics are quantitatively unique to the particular tube under discussion and serve primarily to suggest what is possible with this type of tube. Any decisions to acquire a similar device should be based upon extensive testing of the particular tube under consideration in an effort to determine characteristics peculiar to that tube.

II. THE TUBE

This report contains results of testing on a single stage, magnetically focused I.T.T. model F-4094 (ser. no. 067302) image intensifier. The image tube has a 146 mm photocathode of multi-alkalai extended red type, the spectral response of which appears in Fig. 1. The tube has a 0.4 inch thick quartz photocathode window and a fiber optic output faceplate. An antiscattering baffle in the camera assembly restricts the unvignetted field to a diameter of about 140 mm for our testing purposes.

FIGURE 1

Spectral response of the 140 mm ITT photocathode.

FIGURE 2

P-20 phosphor output spectral distribution

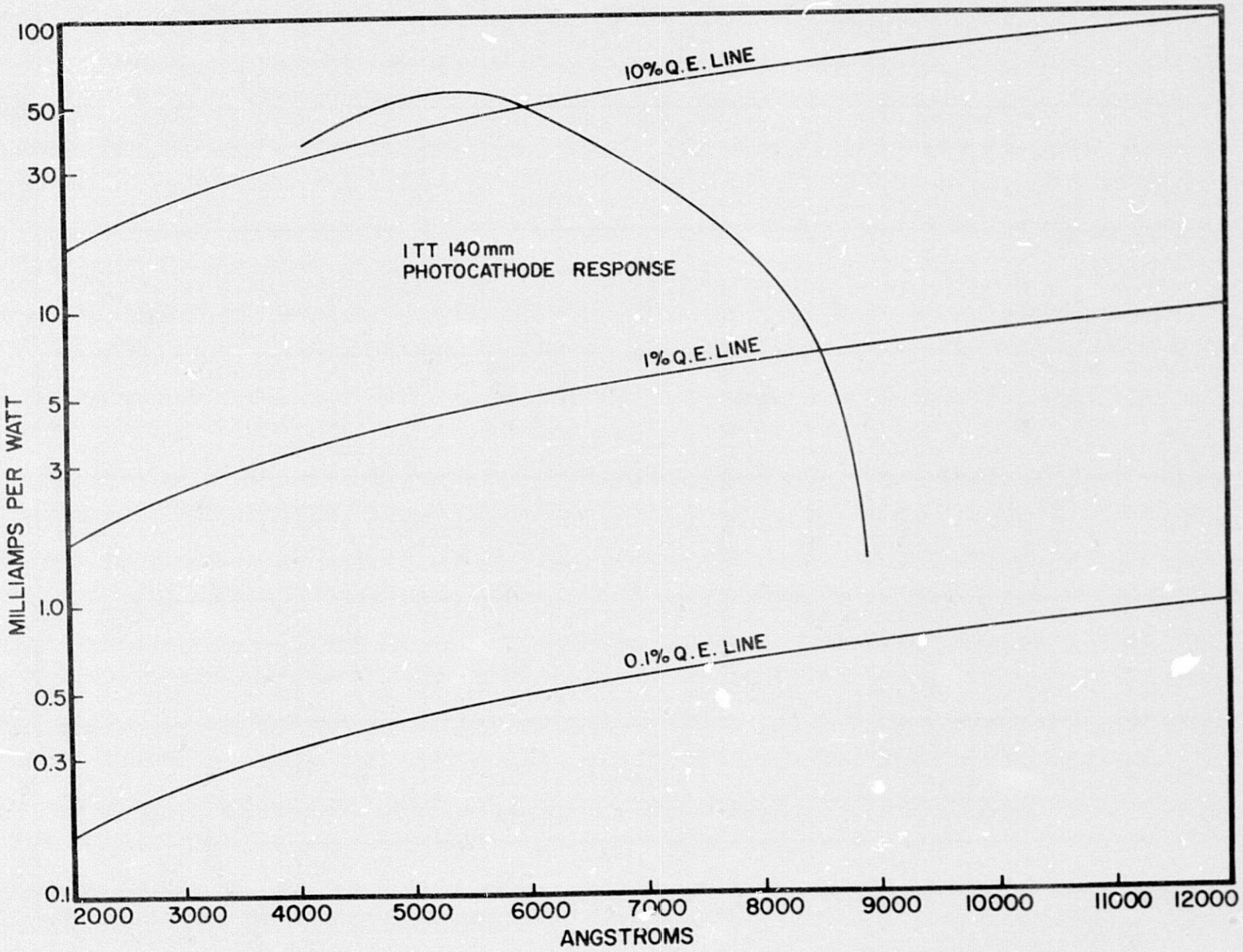
ITT 140mm
PHOTOCATHODE RESPONSE
10% Q.E. LINE
1% Q.E. LINE
0.1% Q.E. LINE
MILLIAMPS PER WATT
100
50
30
10
5
3
1.0
0.5
0.3
0.1
2000
3000
4000
5000
6000
7000
8000
9000
10000
11000
12000
ANGSTROMS

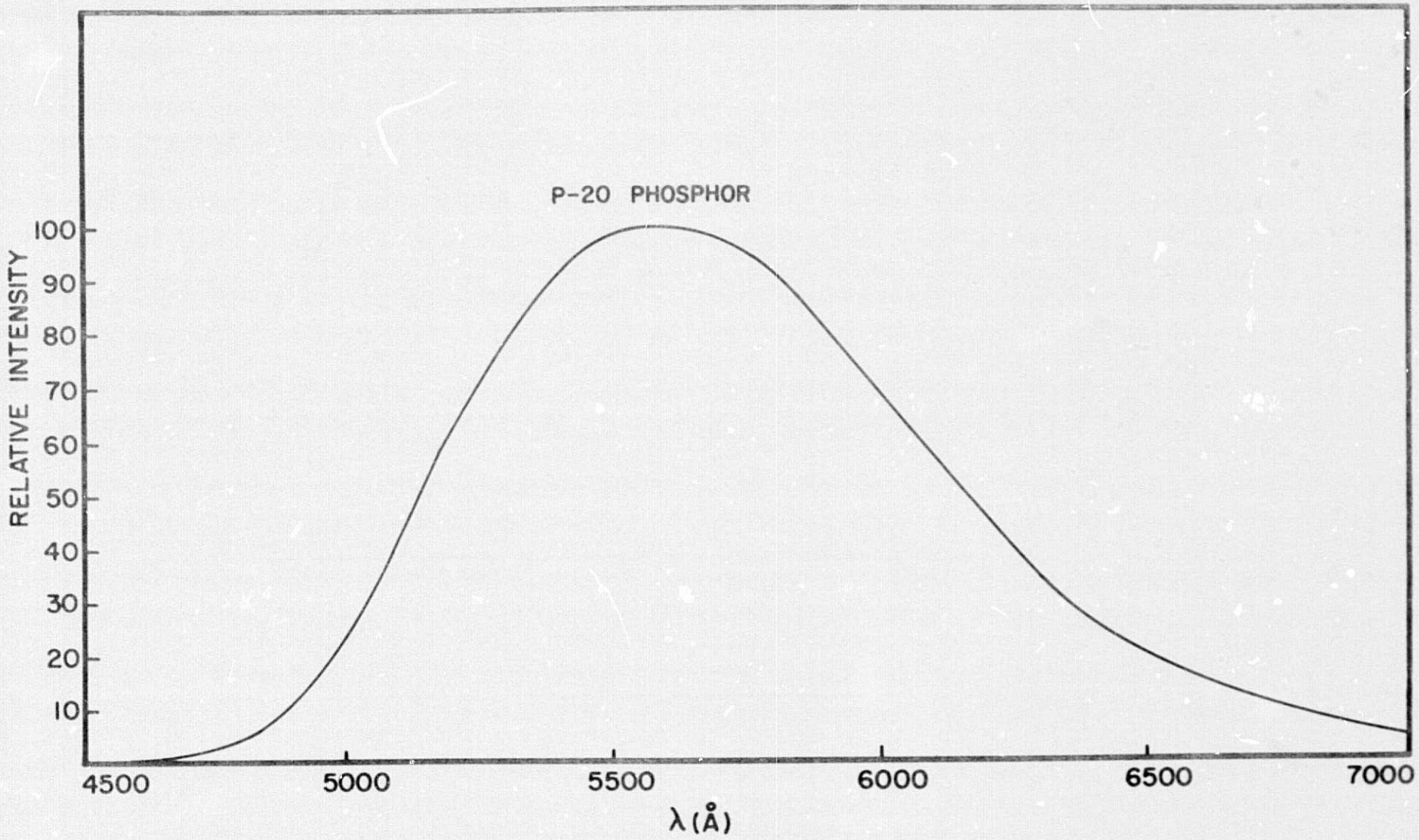
P-20 PHOSPHOR
RELATIVE INTENSITY
100
90
80
70
60
50
40
30
20
10
4500
5000
5500
6000
6500
7000
λ (Å)

The green (P-20) output phosphor generally lends itself to being best photographed with a D sensitized emulsion. The phosphor spectral distribution is indicated in Fig. 2.

A photograph of the tube/camera assembly (Fig. 3) indicates the major components of the system. The subassemblies consist of: (1) a rectangular unit containing two separate filter slides, a dark slide and a focus target projector, (2) a cylindrical unit which houses the image tube, its solenoid and a solenoid cooling jacket. (The cooling jacket has been used with both circulating water and alcohol, generally used to hold the solenoid temperature slightly below ambient temperature) (3) a plate holder slide unit for mounting either a plate holder or an eyepiece unit, (4) a plate holder unit and (5) an eyepiece unit. The eyepiece unit replaces the plate holder when in use. The eyepiece unit is used primarily for fine tuning the focus of the solenoid and for focusing the telescope feed to the image tube by means of visual inspection first of the focus target image and second of a stellar image fed by the telescope.

The plate holder system is composed of a pressure plate plunger assembly which upon removal of a plate holder dark slide permits the plate assembly to be pressed forward against the fiber optic coupling faceplate. This operation must be given some care as the plate/fiber optic contact must be as complete and firm as possible. The system at Steward Observatory has exclusively involved the use of circular, 180mm diameter plates; the application of film and film transports to this system will be discussed in another report.

The camera system with all of its subassemblies has a total weight of about 115 pounds; there is some room for variation in this weight through modification of the filter slide assembly but the bulk of the

FIGURE 3

The 140 mm image tube camera. Indicated subassemblies: A. tube and solenoid housing, B. cooling valves, C. filter carrier box, D. resolution projector slide, E. step wedge projector receptacle, F. plate-holder assembly, G. plate-holder dark slide, H. plate-holder plunger assembly and I. eyepiece unit.

A
B
B
C
D
E
F
G
H
I
J

unit (i.e. solenoid housing and image tube cell) can undergo very little modification short of removal of the solenoid focusing mechanism/cooling jacket with subsequent replacement by a series of permanent magnets.

The cooling system involves a hookup of two tygon tubes to permanently placed valves on the image tube housing. Flow rate of coolant is about 1 liter/minute at about 65°F.

The focus target projector, which slides in and out of the optical path operates on a 5v. DC power supply, the solenoid is operated in the "current mode" at about 7.25 amps and the tube is operated at about 15.5 kv but never over 17 kv. It should be noted that the resolution of the tube is a very sensitive function of the solenoid current and must be fine tuned before each use in order to obtain optimum results.

The camera has been operated with a variety of filter combinations at the 90" telescope; in general it is important not to allow light from a star brighter than V = 6.0 to strike the photocathode unfiltered. When operating with a 1000 Å band pass this value is V~4.5.

The cylindrical assembly of the image tube camera (Fig. 3) is 13" long by 12" diameter; the filter slide box used with this camera is 12" square and about 4" deep.

III. TESTING FACILITIES

The testing of the 140 mm tube was conducted at the Image Tube Laboratory of Steward Observatory. The principal goal of this facility is to determine the extent to which accurate radiometric and positional data may be obtained from an image tube record and to determine the precautions necessary to obtain such data. Most of the tests involve photographing the image tube output which is the most efficient, accurate and convenient method of permanently recording information from an image

intensifier. Most of the data reduction was performed using facilities at Steward Observatory; PDS reductions were performed using facilities at Kitt Peak National Observatory.

IV. EVALUATION OF IMAGE TUBE PROPERTIES

A. Resolving Power

The resolving power of the image intensifier/camera system was evaluated in two ways: (1) a high contrast Baum Resolution Pattern (Fig. 4) was projected on the photocathode and the resultant output was measured visually using a high power (100X) microscope; this procedure yielded the resolving power of the image tube; (2) the Baum Resolution Pattern was also photographed using three different types of emulsions: 103aD, II-J, and IIIaJ. This procedure yielded the resolving power of the image tube with fiber optic coupling to emulsions of different intrinsic resolving powers.

In all cases the projection pattern was centered on the photocathode, the solenoid current was adjusted to optimize resolution at the center of the photocathode and the image of the pattern was then translated across the photocathode in 0.2 inch increments. The portion of the pattern in Fig. 4 which is of interest here is the series of parallel lines and spaces calibrated in equivalent line pairs per millimeter (lp/mm). At each image position on the photocathode a determination was made of the limiting number of line pairs per millimeter that could be visually resolved. In the case of visual measurements both the tangential and the radial limiting resolution were determined where the tangential values were obtained with the resolution pattern perpendicular to the photocathode radius vector. The radial values were obtained for a 90° rotation of the pattern.

FIGURE 4

The Baum resolution projection pattern; frequencies range from 8 to 100 lp/mm and are indicated by numbers above the vertical lines.

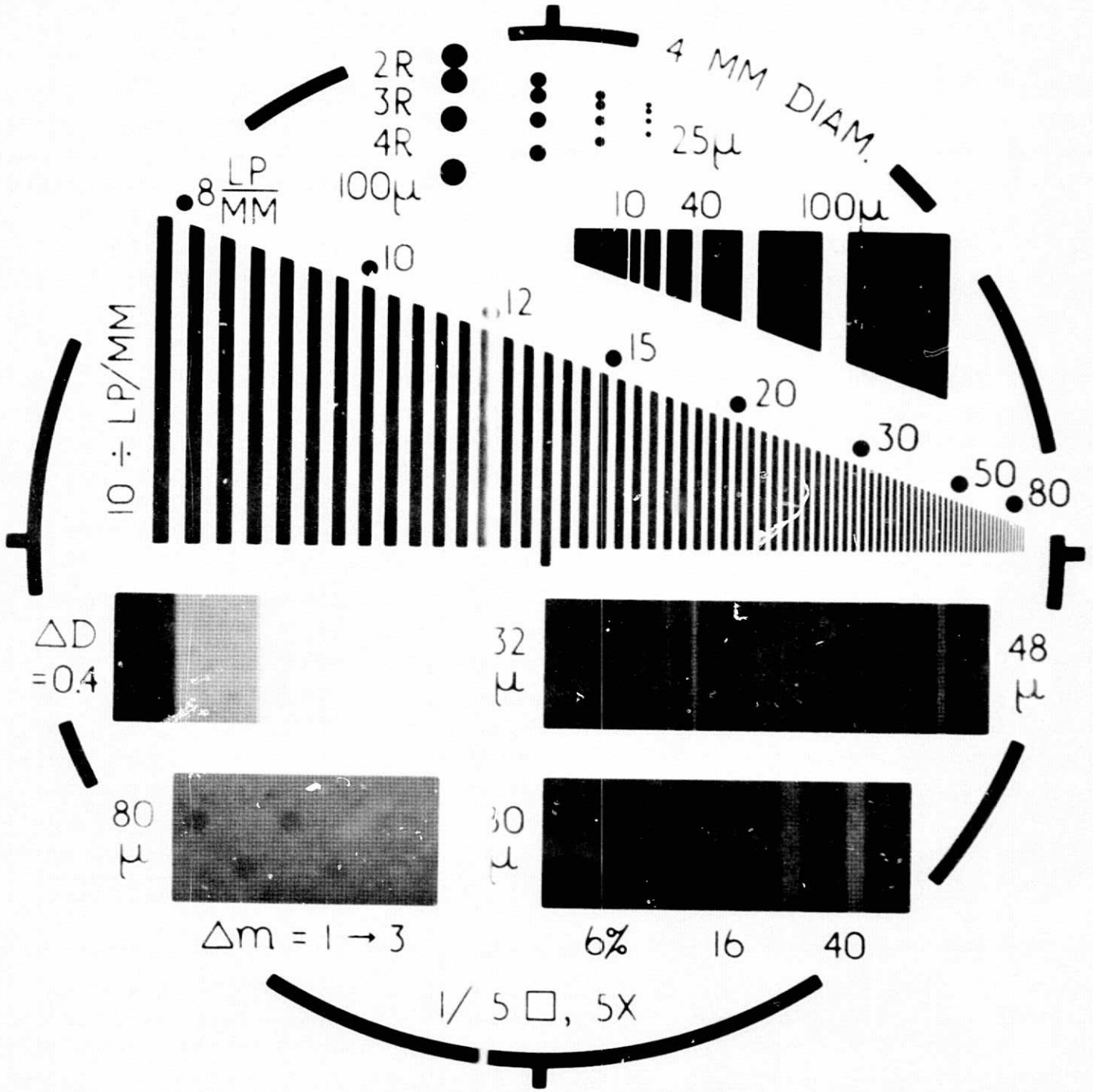
2R
3R
4R
100μ
4 MM DIAM.
25μ
10 40 100μ
8 LP/MM
10
12
15
20
30
50
80
10 ÷ LP/MM
ΔD
=0.4
32
μ
48
μ
80
μ
30
μ
Δm = 1 → 3
6%
16
40
1/ 5 □, 5X

The limiting resolutions obtained by examination of the output phosphor are plotted in Fig. 5. The dashed portion of the curve is an extrapolation which was necessary due to mechanical constraints imposed by the geometry of the camera structure. It should further be noted that the limiting frequencies are greater than those obtained from measurements of images on a variety of photographic emulsions due to the degradation of image inherent in the coupling of phosphor and emulsion.

It is apparent from Fig. 5 that the limiting resolution is substantially lower at the edge of the field than near the center. It should also be recognized that the detailed dependence of resolution on field position can be a strong function of the particular tubes tested and even similar tubes from a specific manufacturer can be expected to vary substantially in resolving power.

The tangential limiting resolution on photographic records was determined by photographing the Baum Projection Pattern at a series of positions across the photocathode. The standard 140mm image tube camera plate holder was used which provided contact between the plate and the filter optic output faceplate by means of a foam rubber pressure pad. Although this technique has produced the most reliably uniform contact between photographic plate and fiber optics it is apparent that this is a difficult problem to be given some attention.

Table 1 lists the photographic emulsions used in this test along with general characteristics taken from Eastman Kodak (1967). The characteristics may be taken as a rough guide although every effort was made to treat these plates as recommended by Kodak. All processing was done with rotating rocker tray agitation in Kodak D-19 developer for 4 minutes at 20°C (68°F).

FIGURE 5

Limiting resolution across the diameter of the 140 mm photocathode. Open circles refer to tangential resolution; closed circles are for radial resolution. The finely dotted line indicates that the resolution was in excess of the 100 lp/mm measurable with the Baum resolution pattern. Dashed lines are extrapolations to the extreme edge of the photocathode.

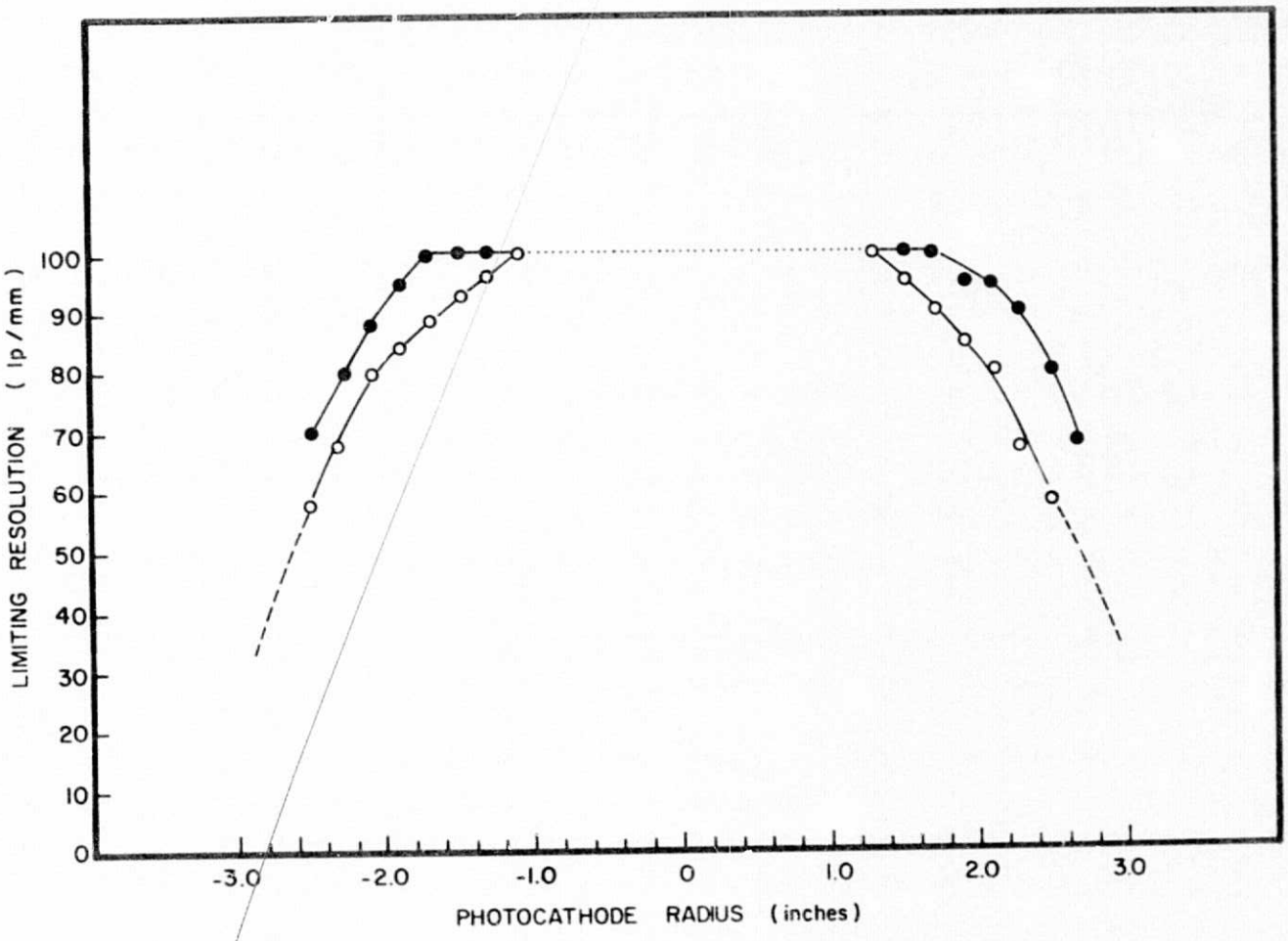
LIMITING RESOLUTION (lp / mm)
100
90
80
70
60
50
40
30
20
10
0
-3.0
-2.0
-1.0
0
1.0
2.0
3.0
PHOTOCATHODE RADIUS (inches)

Table 1

Designation	Spec. Sensitization	Speed	Contrast	Resolving Power	Granularity
103aD	yellow-red	fast	medium	moderately	moderately course
IIaD	yellow-red	fast	medium	medium	medium
IIIaJ	blue-green	moderately fast	high	very high	very fine

The photographic results have been represented by plotting the limiting resolution of the photographic records as a function of the limiting resolution of the image tube output phosphor. In order to accomplish this the resolution data were corrected for magnification by the image intensifier (see following section).

For the tangential orientation

$$R_{phos} = R/M_i$$

where R is the limiting resolution of the image tube phosphor output, M_i is the incremental magnification and R_{phos} is the limiting resolution expressed as spatial frequencies on the output side. An identical relationship exists for the photographic case

$$R_{pg} = R/M_i$$

where R is the photgraphic resolution expressed in terms of the input photocathode image.

Fig. 6 gives the result of plotting the limiting photographic resolution, R_{pg}, versus the limiting phosphor resolution, R_{phos} for the three types of emulsions used on this test. Because of the rather high and comparatively uniform limiting resolution across this particular tube the indicated range of limiting resolutions is rather small. In addition, as noted from Fig. 4, the R_{phos} of the tube is very high, greater than

100 lp/mm over a large portion of the tube, and could not be quantitatively measured with the Baum Resolution Pattern. To accommodate this difficulty we have noted three points in Fig. 6 beyond R_{phos} = 100 lp/mm. These points indicate the maximum values of R_{pg} for each emulsion tested. These points (1, 2 and 3) indicate R_{pg} (max) equals 30 lp/mm for 103aD, 33 lp/mm for IIaD and 43 lp/mm for IIIaJ emulsions.

The lower resolution of the fiber optically coupled photographs is largely due to the difficulty of achieving complete contact between emulsion and fiber optic output faceplate. This difficulty arises from microscopic and macroscopic warping of the glass plates supporting the emulsion and is probably a problem for which there is no adequate solution as long as glass plates are used. It is anticipated that the application of emulsion on film may help resolve this problem. A more complete discussion of the problem of glass plate/fiber optic faceplate contacting may be found in Cromwell and Dyvig (1973).

B. Geometrical Characteristics

The geometrical properties of the 140mm image tube have been examined by measurement of a grid pattern photographed by 103aD emulsion at a tube voltage of 15.5 kv. (Fig. 7). The pattern consists of a series of radii with indicated position angles; eight of the radii have been divided into thirty five smaller segments. Each division serves as a test point for measurement. We have used this pattern to evaluate two characteristics of the tube; the magnification and the incremental magnification.

Magnification is defined as the ratio of the measured radial distance of a test point in the output to the corresponding radial distance in the input. The magnification data points are the mean values obtained from

FIGURE 6

R_{pg} vs. R_{phos} for the 140 mm image tube camera and three emulsions. Points 1,2 and 3 (see text) refer to the limiting R_{pg} for each emulsion.

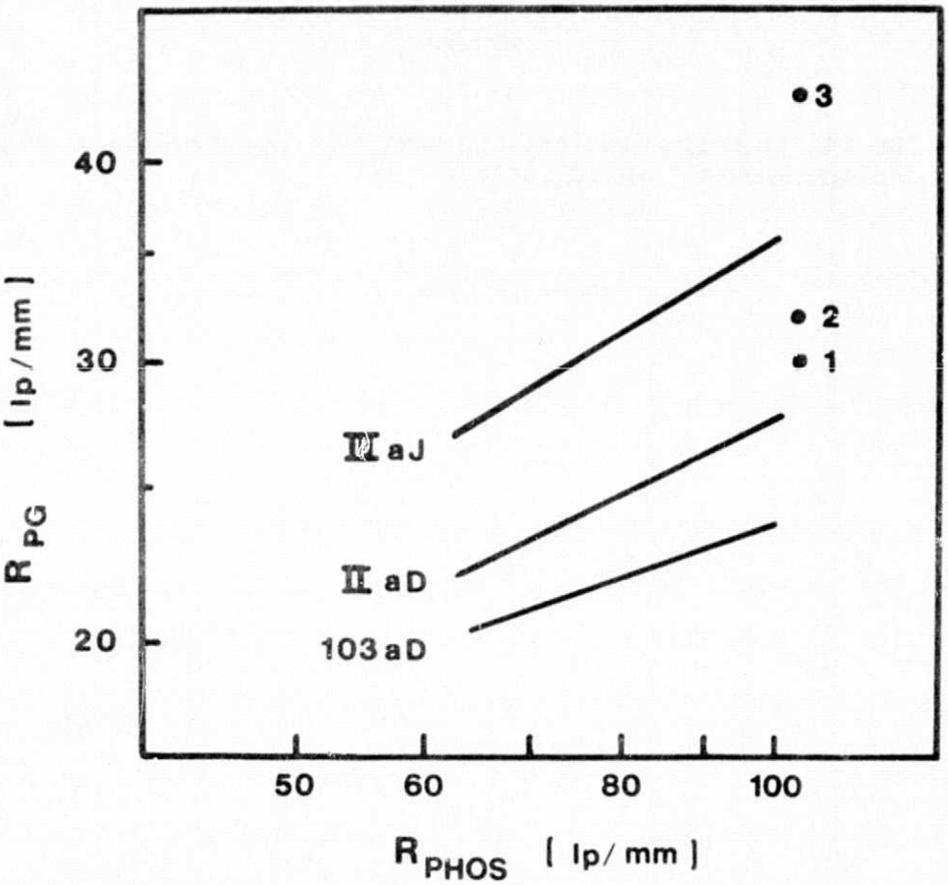
40
30
20
R PG (lp/mm)
IIIaJ
IIaD
103aD
3
2
1
50
60
80
100
R PHOS (lp/mm)

FIGURE 7

The radial projection pattern used for measurements of magnification and incremental magnification.

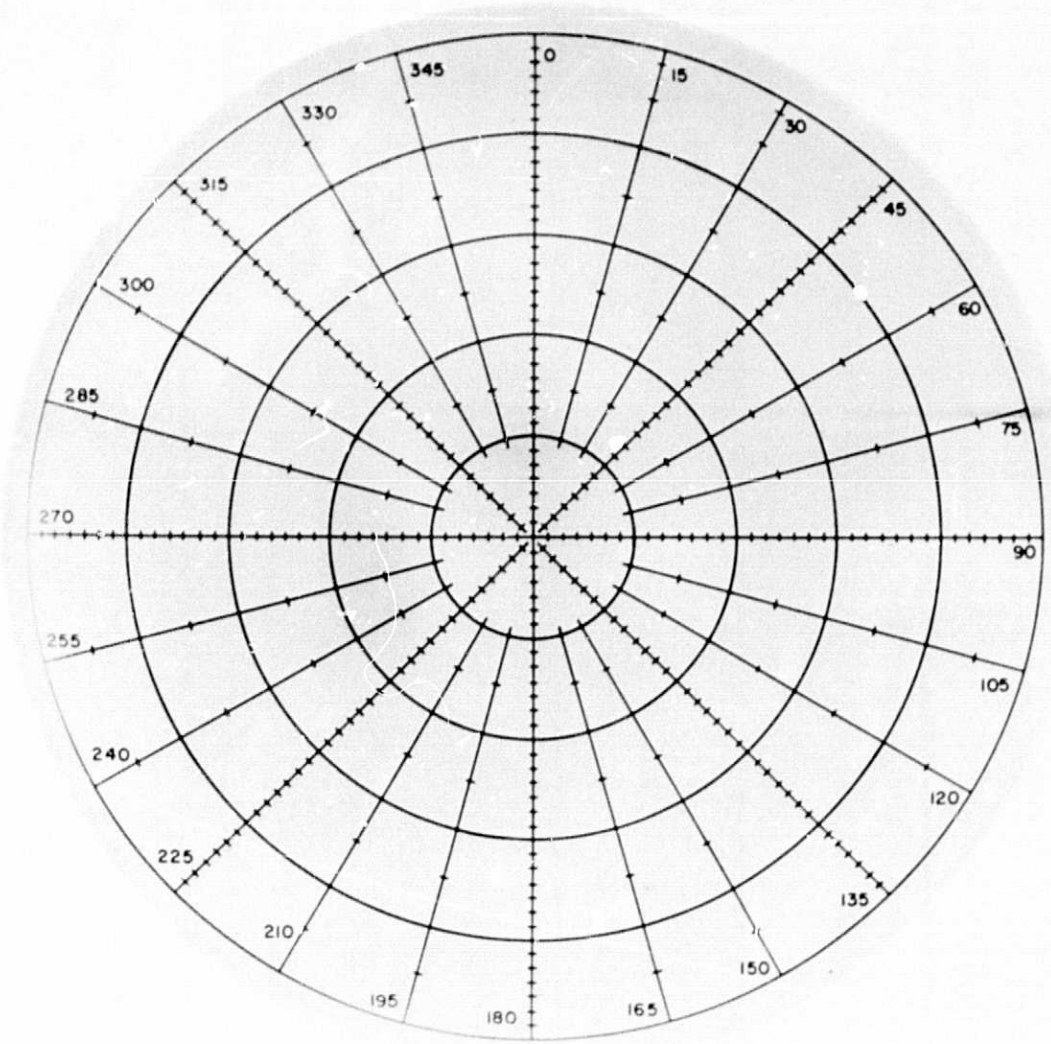
0
15
30
45
60
75
90
105
120
135
150
165
180
195
210
225
240
255
270
285
300
315
330
345

measurements along four radii at position angles 0^{o}, 90^{o}, 180^{o} and 270^{o}. The data points have been grouped into lines corresponding to 8mm increments in the photocathode radius in an effort to reduce the scatter caused by random errors in measurement. These data are plotted in Fig. 8 as magnification versus photocathode radius. Because it was impossible to measure the input grid size on the photocathode it was necessary to make all input measurements on the much smaller projection pattern on the input side. The result was the necessity of normalizing the resultant data. This normalization process probably largely accounts for the degree of curvature and larger scatter of points near the center of the photocathode. In any case these data indicate a remarkably constant magnification across the tube. The great uniformity of this result can best be appreciated by comparison with the magnification of other types of tubes tested at the Steward Observatory facility (Cromwell and Dyvig 1973).

Incremental magnification is defined as the output to input ratio of the radial separation of the test points indicated above. As in the case of determination of magnification the x and y coordinates of the test points were obtained by measurements on a two-coordinate Grant measuring engine for each of four radii at position angles 0^{o}, 90^{o}, 180^{o} and 270^{o}. The incremental magnification for each radius is plotted separately in Fig. 9 again in bins of 8mm of photocathode radius. The normalization scatter again requires extrapolation of those curves through the zero point. The marked decrease in incremental magnification at the edge of the field is due in part to difficulties in making accurate measurements of the grid at this position and in part to the S-distortion of the tube. However, again this result is remarkably uniform in comparison with the incremental magnification of previously listed tubes. A

FIGURE 8

Magnification versus photocathode radius.

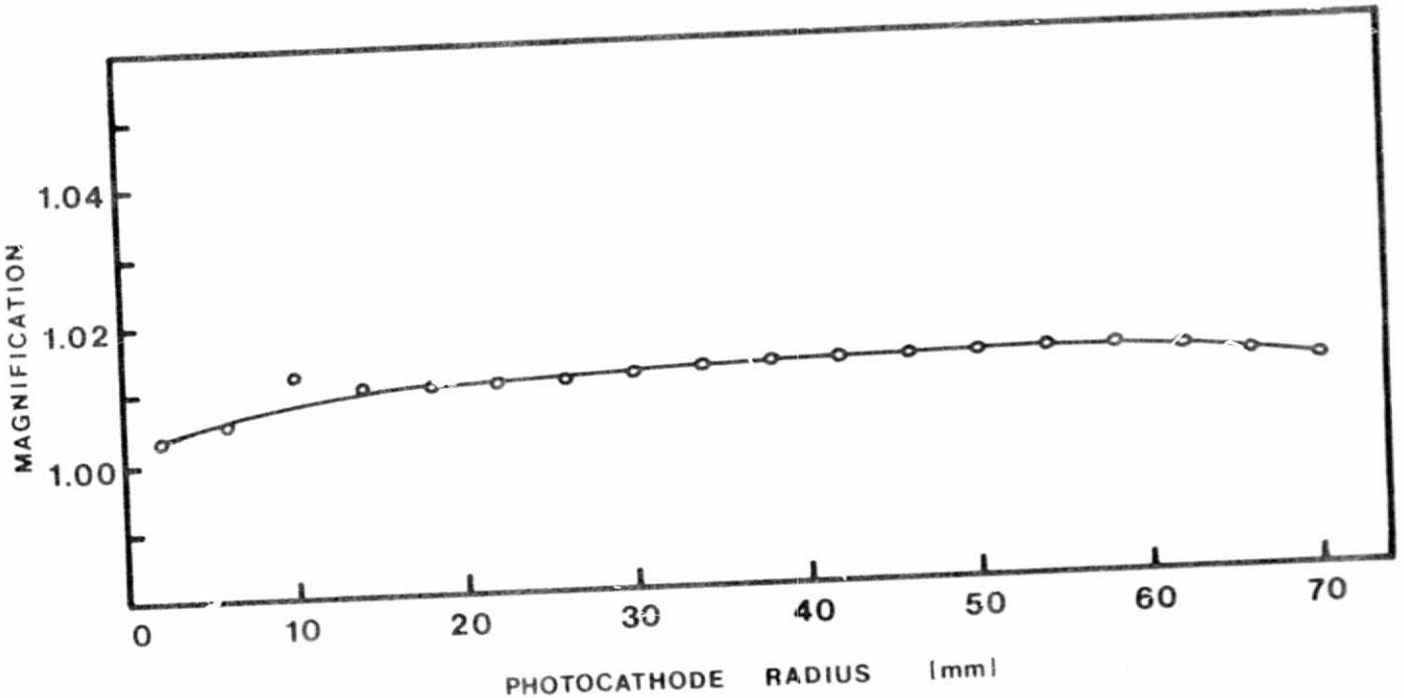
MAGNIFICATION
1.04
1.02
1.00
0
10
20
30
40
50
60
70
PHOTOCATHODE RADIUS [mm]

FIGURE 9

Incremental magnification vs. photocathode radius at four different position angles as follows: crosses for 0° , squares for 90° , circles for 180° and triangles for 270° .

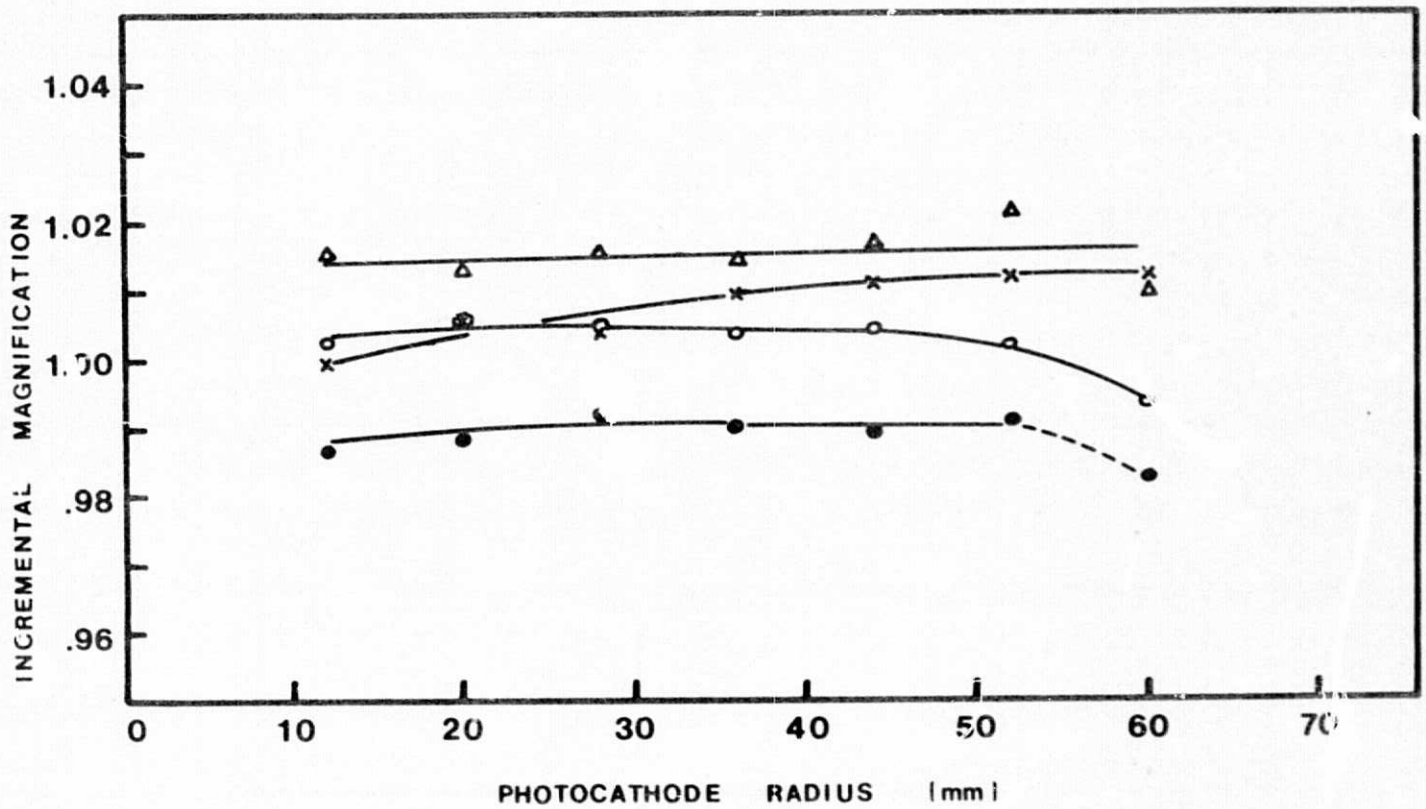
1.04
1.02
1.00
.98
.96
INCREMENTAL MAGNIFICATION
0
10
20
30
40
50
60
70
PHOTOCATHODE RADIUS (mm)

comparison with results for other tubes (Cromwell and Dyvig 1973) indicates that the y axis scale is greatly expanded in Fig. 9 giving a false impression of large variations in incremental magnification. Were these results plotted on a similar scale the incremental magnification curves would merge into a single nearly straight line.

The S-distortion, a characteristic of magnetically focused tubes, is defined as the deviation from a radial axis of a straight line (input) that passes through the center of the field. Mean values of S-distortion have been obtained by measurement of a Ronchi ruling pattern photographed through the image tube. The results of this measurement are plotted in Fig. 10.

For some applications the S-distortion can be a troublesome problem and must be dealt with. In many cases the S-distortion can be adequately determined and appropriate corrections can be applied to the data. There may however, be applications where very high positional accuracy is required and in this event a detailed calibration of the image tube geometry will be essential.

We also note that the geometric distortions are highly dependent upon the magnetic field and may show large variations as a function of the positioning of the focusing magnets.

C. Fiber Optic Faceplate Shear

Fiber optic shear is the displacement which may arise at the interfaces of fiber optic bundles in filber optic faceplates. This shear can adversely affect accurate measurement of positions on plates taken with fiber optically coupled image intensifiers. Several examples of fiber optic shear in the faceplate of the 140mm tube are shown in Fig. 11. The bundles are hexagonal in shape with each side of the bundle about 0.6mm in length.

FIGURE 10

Mean S-distortion vs. photocathode radius.

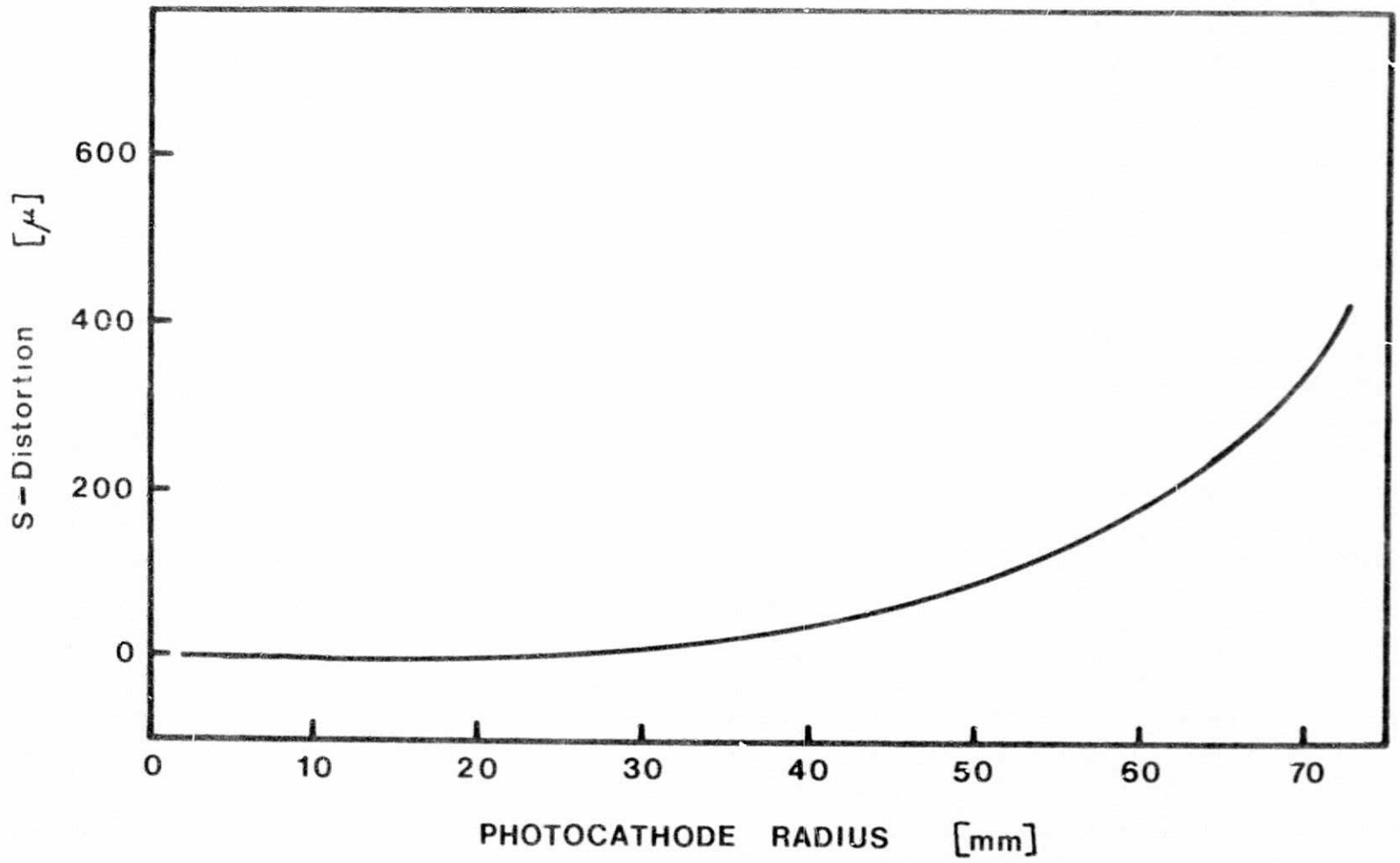
S-Distortion [μ]
600
400
200
0
0
10
20
30
40
50
60
70
PHOTOCATHODE RADIUS [mm]

FIGURE 11

Segment of a Ronchi ruling image obtained with the fiber optic faceplate. Fiber optic shears appear as discontinuities in the rulings; careful examination reveals the hexagonal fiber bundle pattern.

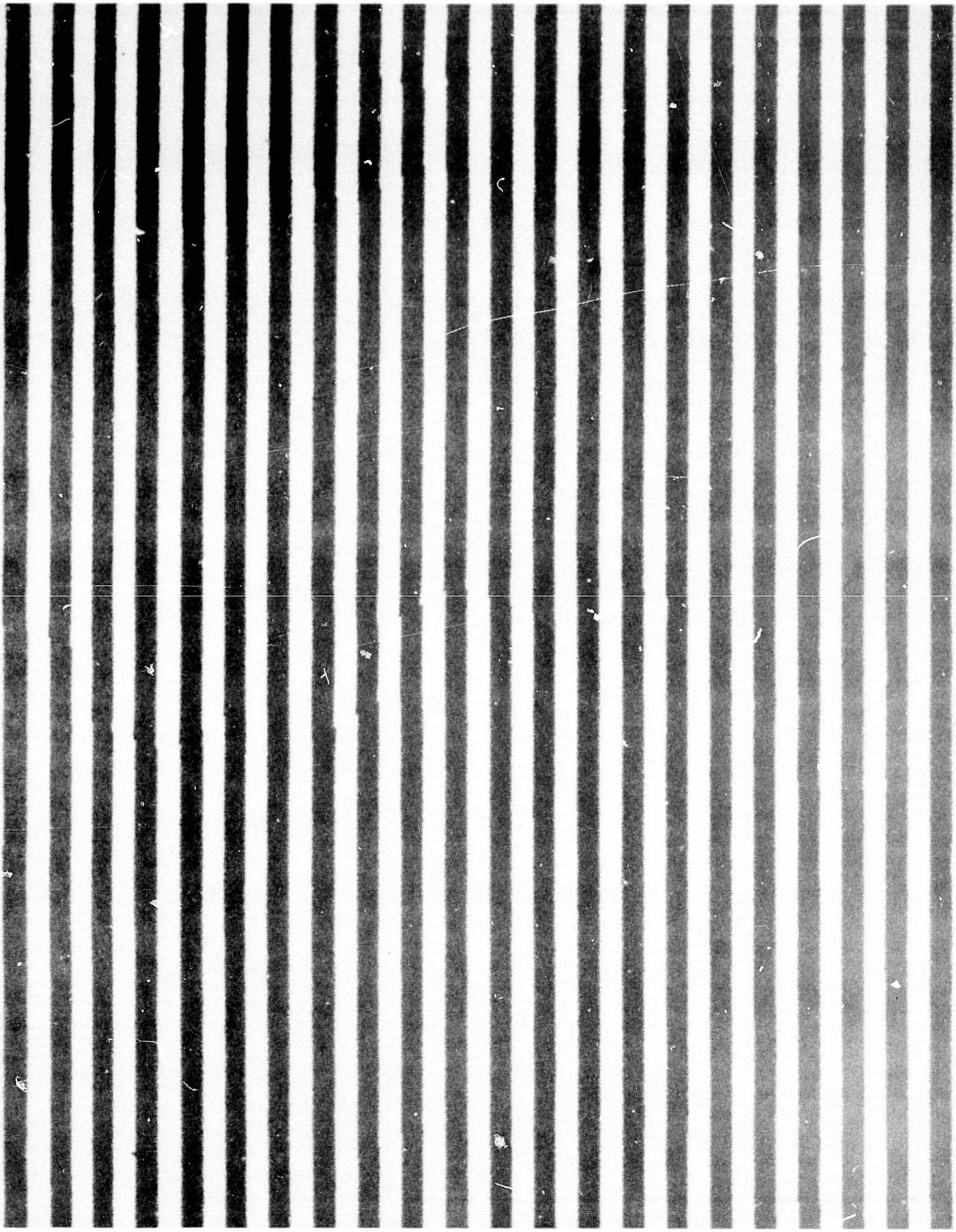

The extent of the shear problem was evaluated by contact photography of a 250 lp/inch Ronchi ruling through the 156mm diameter faceplate. The data were recorded on IIIaJ film at two position angles 45° apart. The photographs were enlarged by a factor of ten and examined for shears which appeared as breaks in the ruling. By combining the results from the two position angle plates it was possible to identify all of the shears to a limit of about 6μ displacement.

The fiber optic shears are most often produced by a displacement along an entire side or sides of the hexagonal array of bundles. These displacements were measured for several one cm^2 regions randomly distributed across the faceplate in order to arrive at a size distribution of the shears. Thes size distribution is uniform, however, shears smaller than 6μ could not be quantitatively measured or even identified. Thus, the total number of bundle interfaces ($\sim$ 41,340) minus the total number of detected shears ($\sim$3,350) is taken to represent the total number of bundle interfaces with zero shear (where zero shear is understood to mean a shear distribution of 0-6μ). These figures indicate that 91.9% of the bundle interfaces have unmeasurable shears of less than 6μ displacement. Identifiable shears (i.e. >6μ) occur at a frequency of about 20 shears/cm^2.

The size distribution of fiber optic shears is indicated in Fig. 12. The largest observed shears are 29μ in size, just about the resolution limit of the camera system. It should be recalled that the shear displacement occurs primarily at the bundle interfaces and does not represent a relative shift of the entire bundle. In most instances it is not expected that fiber optic shear will present a serious difficulty. It should also be noted that the present facplate is representative of the best faceplates currently available.

FIGURE 12

Fiber optic shear size distribution as a percentage of interfaces showing shear vs. shear size (D) in microns. The bar at D=2μ represents all shears between 0 and 6 microns in size.

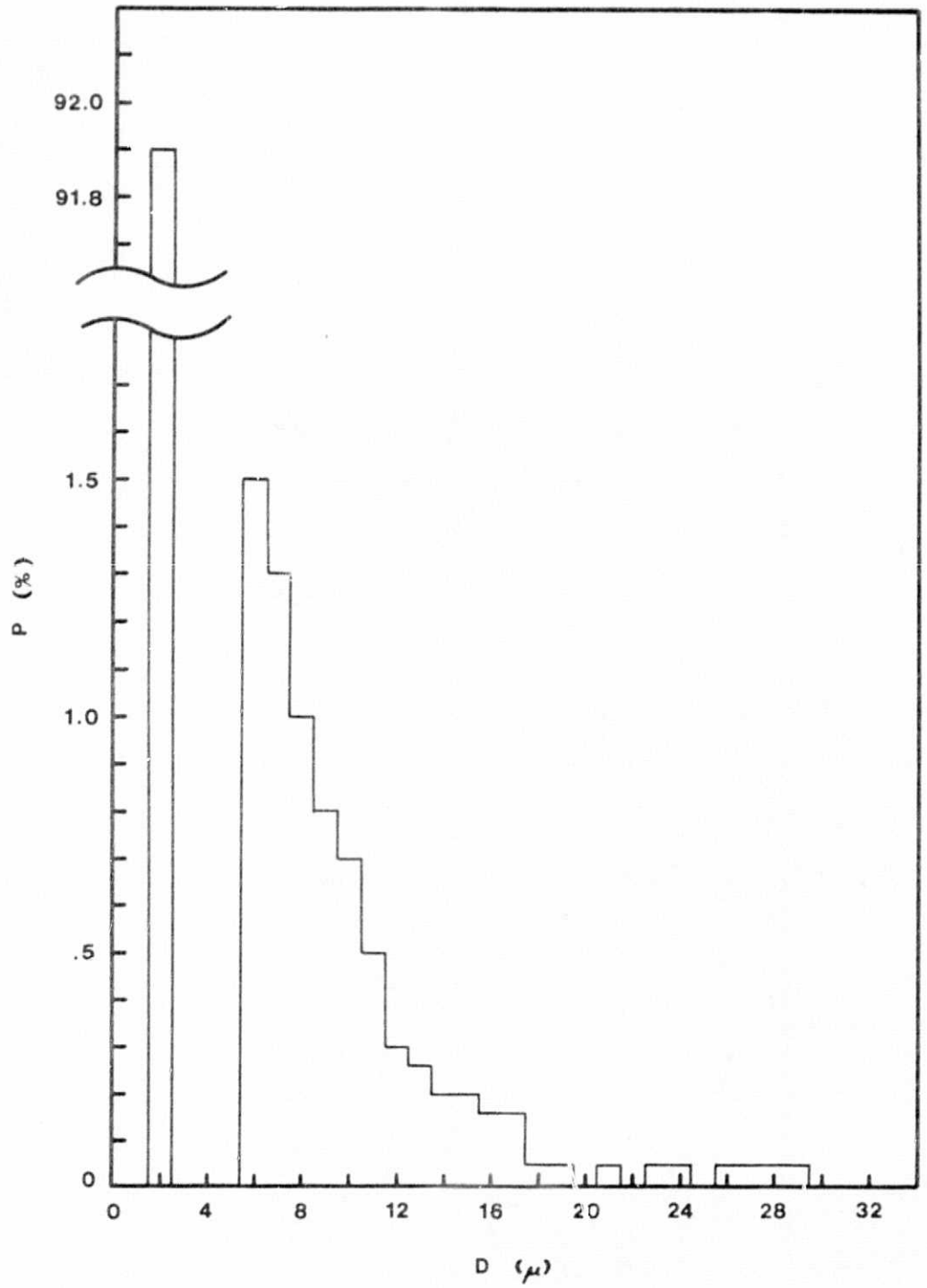
92.0
91.8
1.5
1.0
.5
0
P (%)
0
4
8
12
16
20
24
28
32
D (μ)

D. Uniformity of Response

Uniformity of response of the intensifier output was evaluated by uniformly irradiating the photocathode and recording the resultant output on fine grain photographs (IIIaJ emulsion). Uniform irradiance was provided by a distant point source projector which consists of an incandescent lamp, a defining aperture and a diffuser. Interference filters of abut 250Å FWHM and central wavelengths of 3500Å, 8000Å and 9019Å were used to define four spectral passbands.

Figures 13-16 show photographic records of the output associated with each spectral band. Several characteristic nonuniformity patterns are apparent: 1) a general enhanced or reduced response in localized but rather large regions, 2) a large, rather linear region of enhanced response, particularly apparent with the 9019Å filter and 3) the hexagonal small scale patterns of the fiber optic bundles.

Each of the plates have been scanned with 40μ square apertures in 40μ intervals along three diameters of the plate spaced at 30° intervals in position angle. These density scans have been converted to intensity scans by reference to a calibration plate generated H-D curve. The scans have been deliberately left unsmoothed to indicate fine scale variations due to fiber optic bundles and plate noise. Three scans for each of the four spectral bands appear in Figs. 17-20. A vertical bar in each figure indicates the magnitude of a one percent variation in intensity. At shorter wavelengths the response is extremely uniform, exhibiting less than 1% variations. The nonuniformity of the output increases noticeably on the 9019Å plate but is still on the order of a few percent (2%-3%).

FIGURE 13

Uniformity of response plate at 3500Å.

FIGURE 13

Uniformity of response plate at 3500Å.

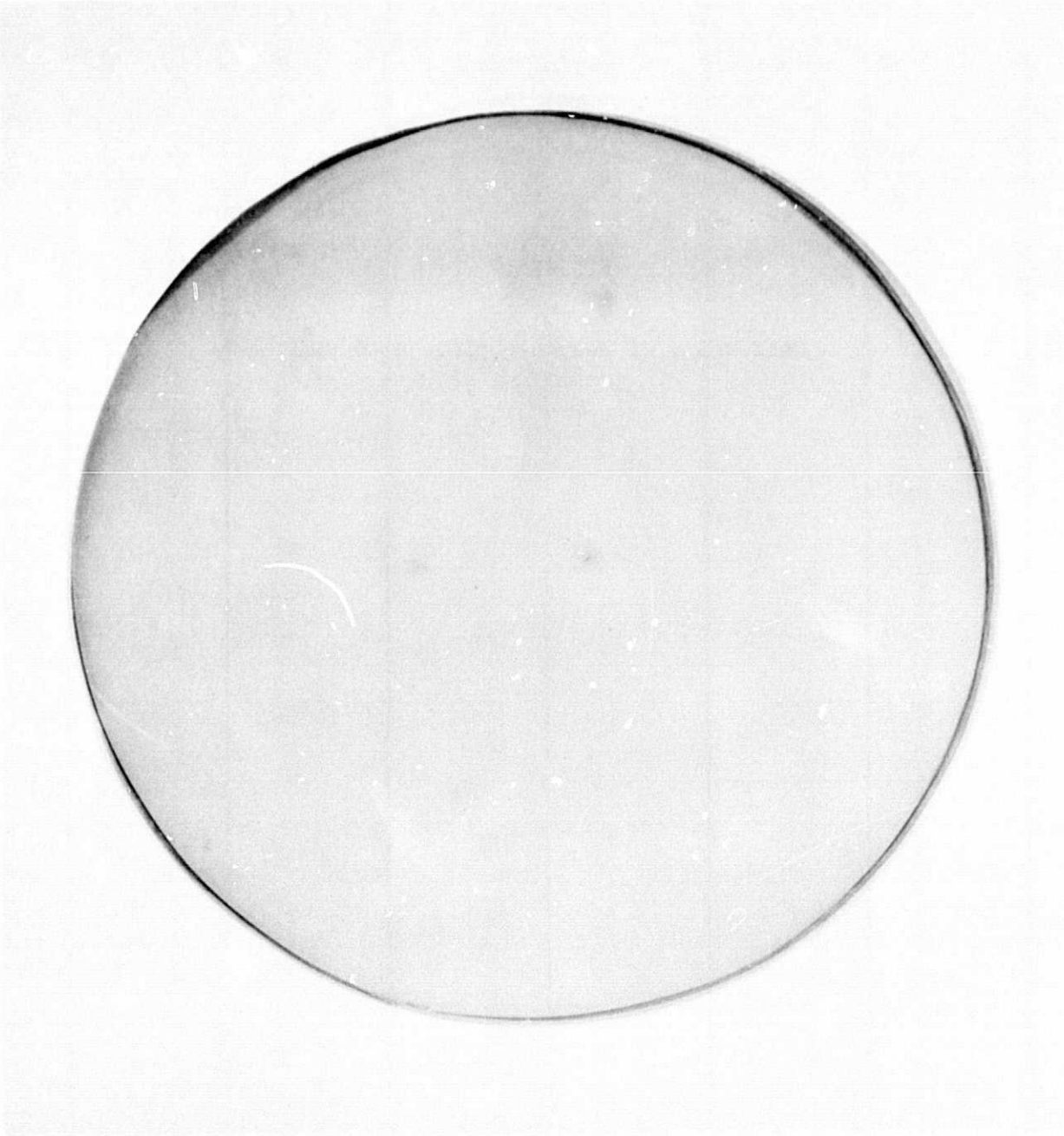

FIGURE 14

Uniformity of response plate at 6500Å.

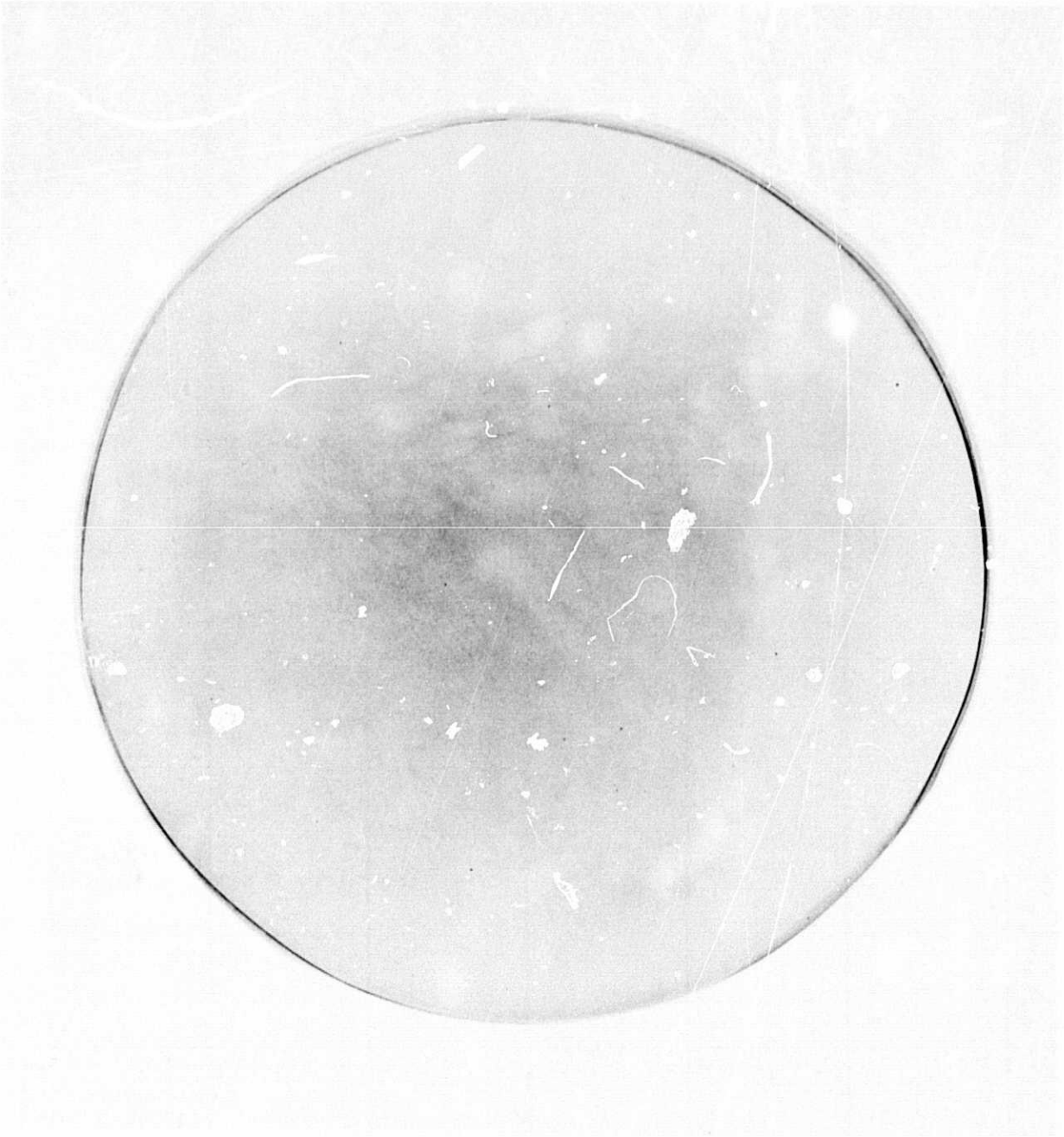

FIGURE 15

Uniformity of response plate at 8000Å.

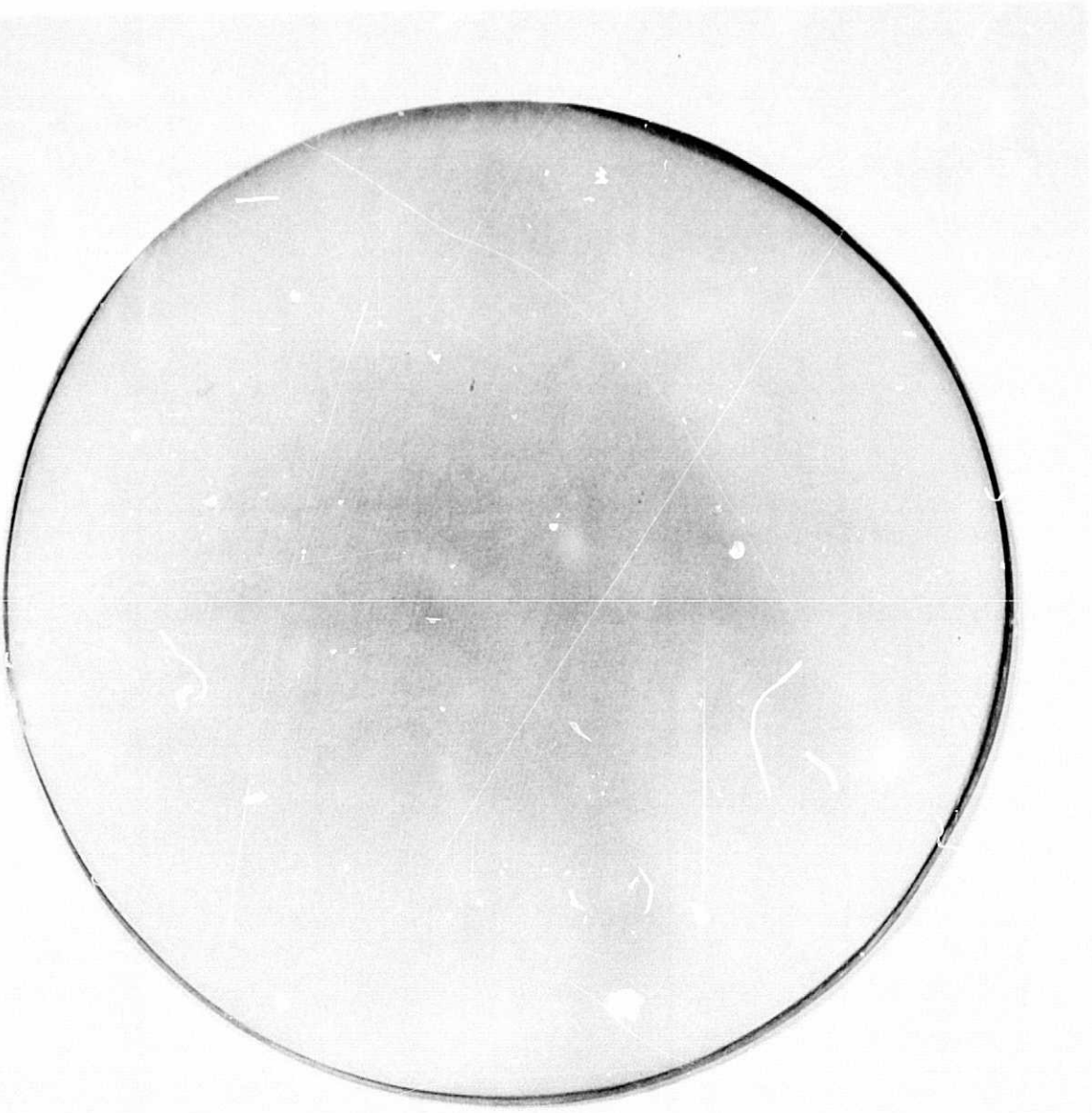

FIGURE 16

Uniformity of response plate at 9019Å.

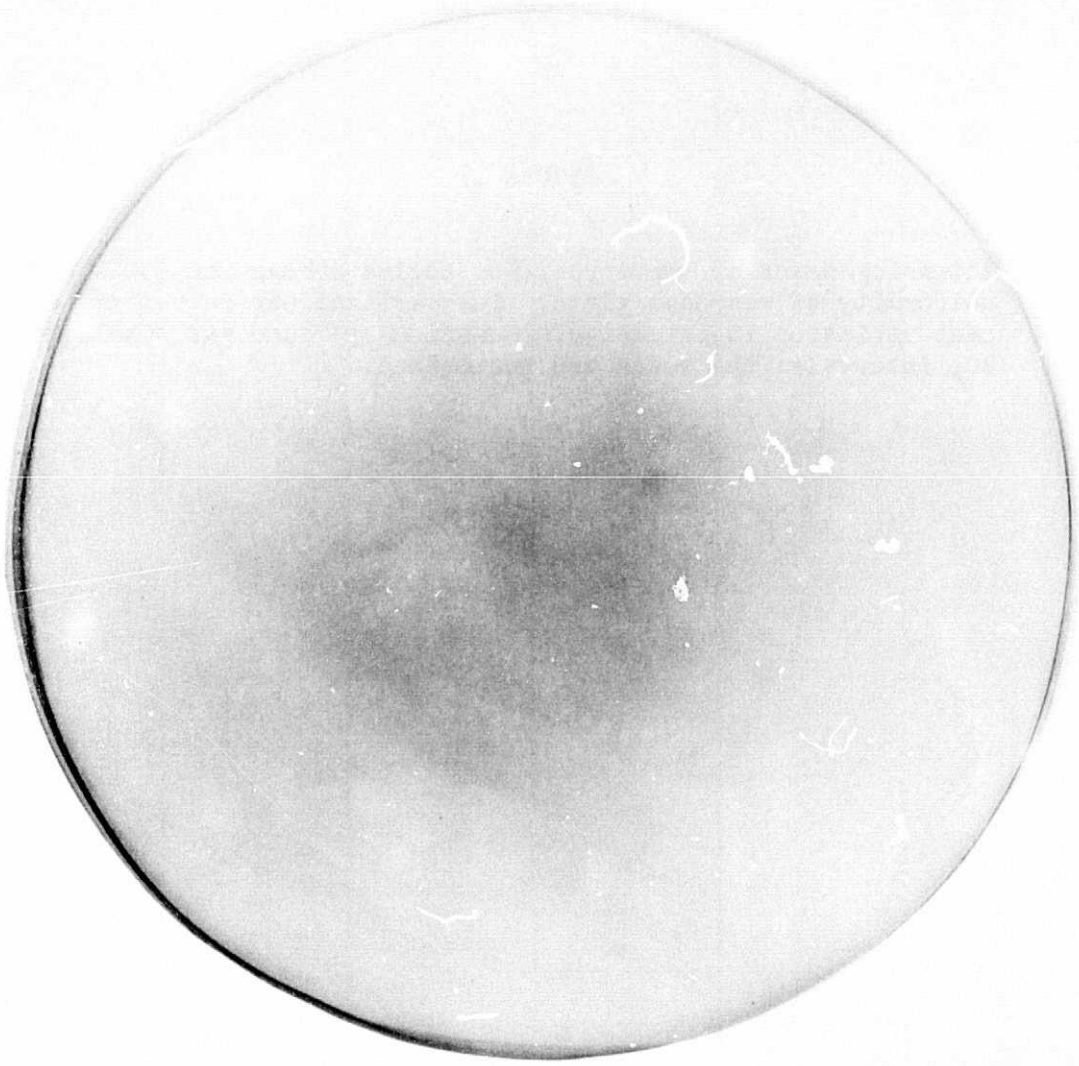

FIGURE 17

Intensity scans at three position angles across the 3500A wavelength uniformity of response plate. The vertical bar represents a one percent variation in intensity. Scanning aperture was 40x40μ stepped in 40μ intervals; the scans are unsmoothed.

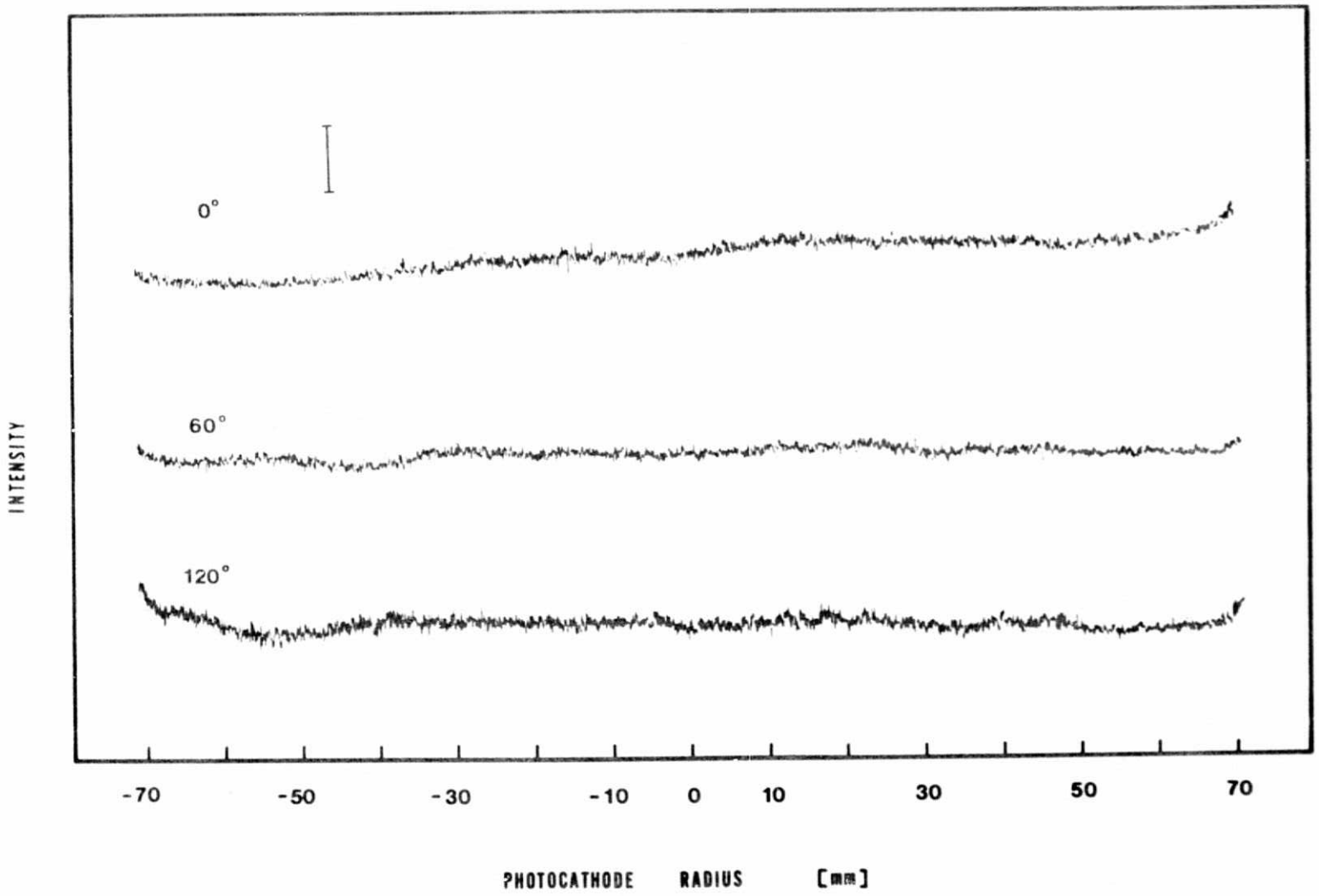
0°
60°
120°
INTENSITY
-70
-50
-30
-10
0
10
30
50
70
PHOTOCATHODE RADIUS [mm]

FIGURE 18

Same as Fig. 17 but for wavelength 6500Å.

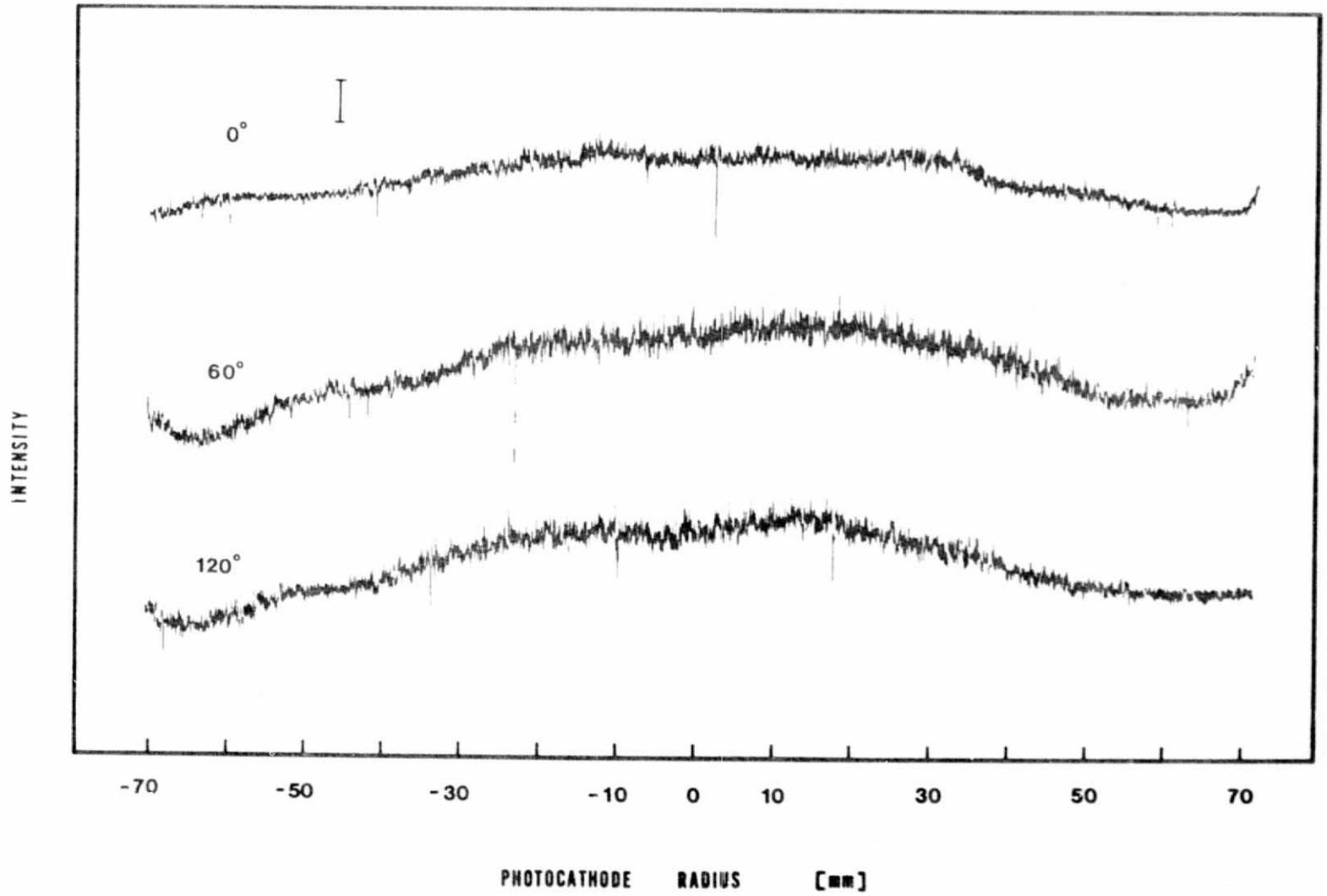
0°
60°
120°
INTENSITY
-70
-50
-30
-10
0
10
30
50
70
PHOTOCATHODE RADIUS [mm]

FIGURE 19

Same as Fig. 17 but for wavelength 8000Å.

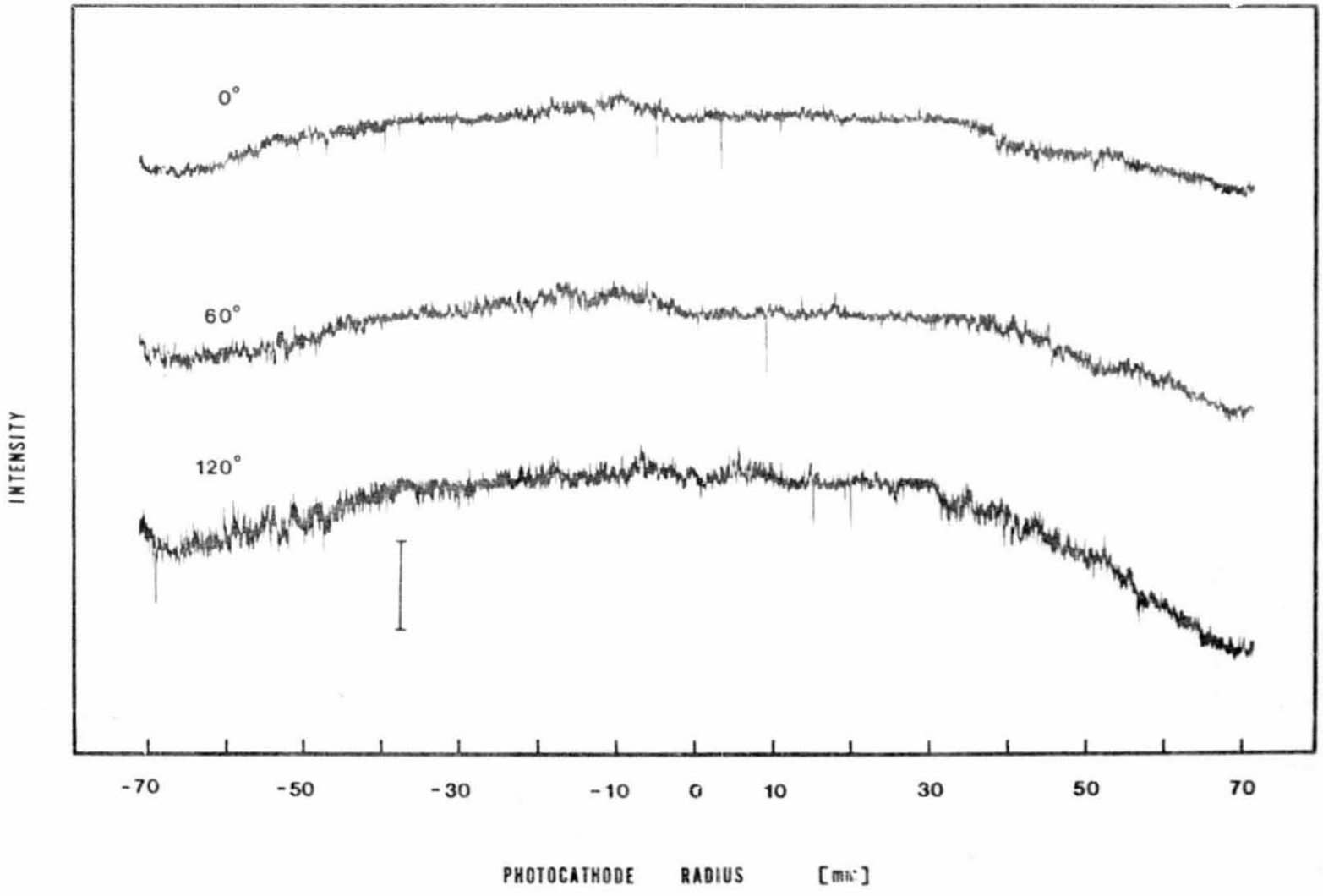
0°
60°
120°
INTENSITY
-70
-50
-30
-10
0
10
30
50
70
PHOTOCATHODE RADIUS [mm]

FIGURE 20

Same as Fig. 17 but for wavelength 9019Å.

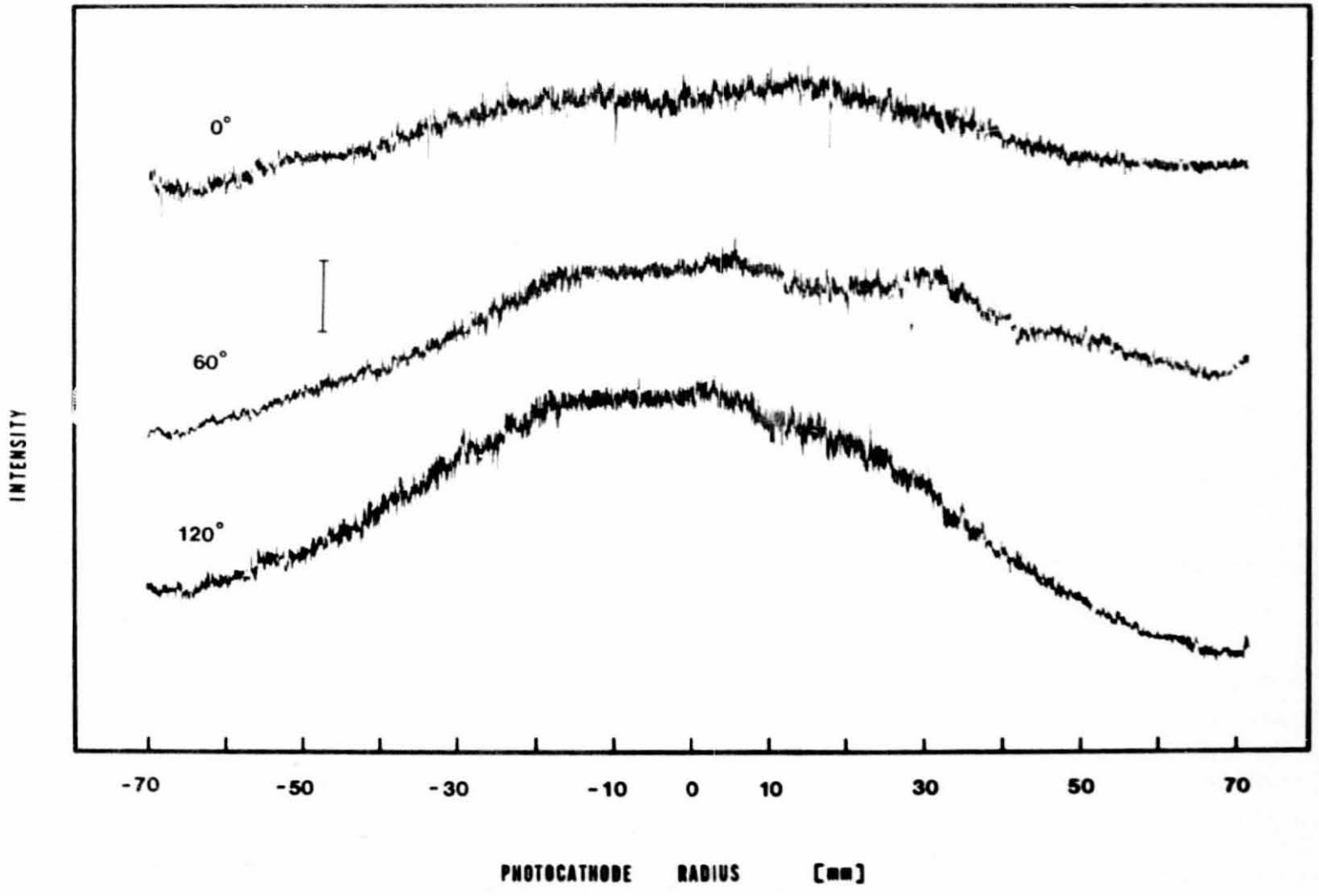
0°
60°
120°
INTENSITY
-70
-50
-30
-10
0
10
30
50
70
PHOTOCATHODE RADIUS [mm]

The nonuniformities of these plates can be subtracted from astronomical plates by use of a PDS area scanner if necessary but this is a rather time consuming and laborious process and should generally be avoided if possible.

A detailed discussion of the causes of different types of nonuniformities can be found in Cromwell and Dyvig (1973).

E. Signal Induced Background

Signal induced background was evaluated by a series of half field tests. Slightly less than half of the photocathode area was uniformly irradiated by a distant point source; the remaining area was masked off using the dark slide. The wavelengths of the incident radiation were 3500Å, 8000Å and 9019Å defined by filters previously described.

Figure 21 shows a typical photograph obtained in the half field test. Density scans were made along a diameter of the field parallel to the edge of the masked portion of the field. These scans were converted to intensity scans and appear in Fig. 22.

There is clearly a strong field dependence for signal induced background which makes it very difficult to properly account for this effect. The degree of the effect can likewise vary over a large range and must be carefully examined for each individual tube.

F. Dark Emission

A record of the dark emission of the tube was made by exposing a IIaD plate for one hour to the phosphor output while the intensifier was in complete darkness. The tube operating voltage was 15.5kv with an ambient temperature of 68°F. A PDS density scan of the plate indicates a mean density above fog of 0.16 with very low scatter. There were no ion events discernable on the plate.

FIGURE 21

Signal induced background at 6500Å as obtained from a half-field test. This is a negative print; the blackened area is heavily overexposed and is the area which was not obscured on the photocathode. The much lighter area shows a response pattern due in part to signal induced noise.

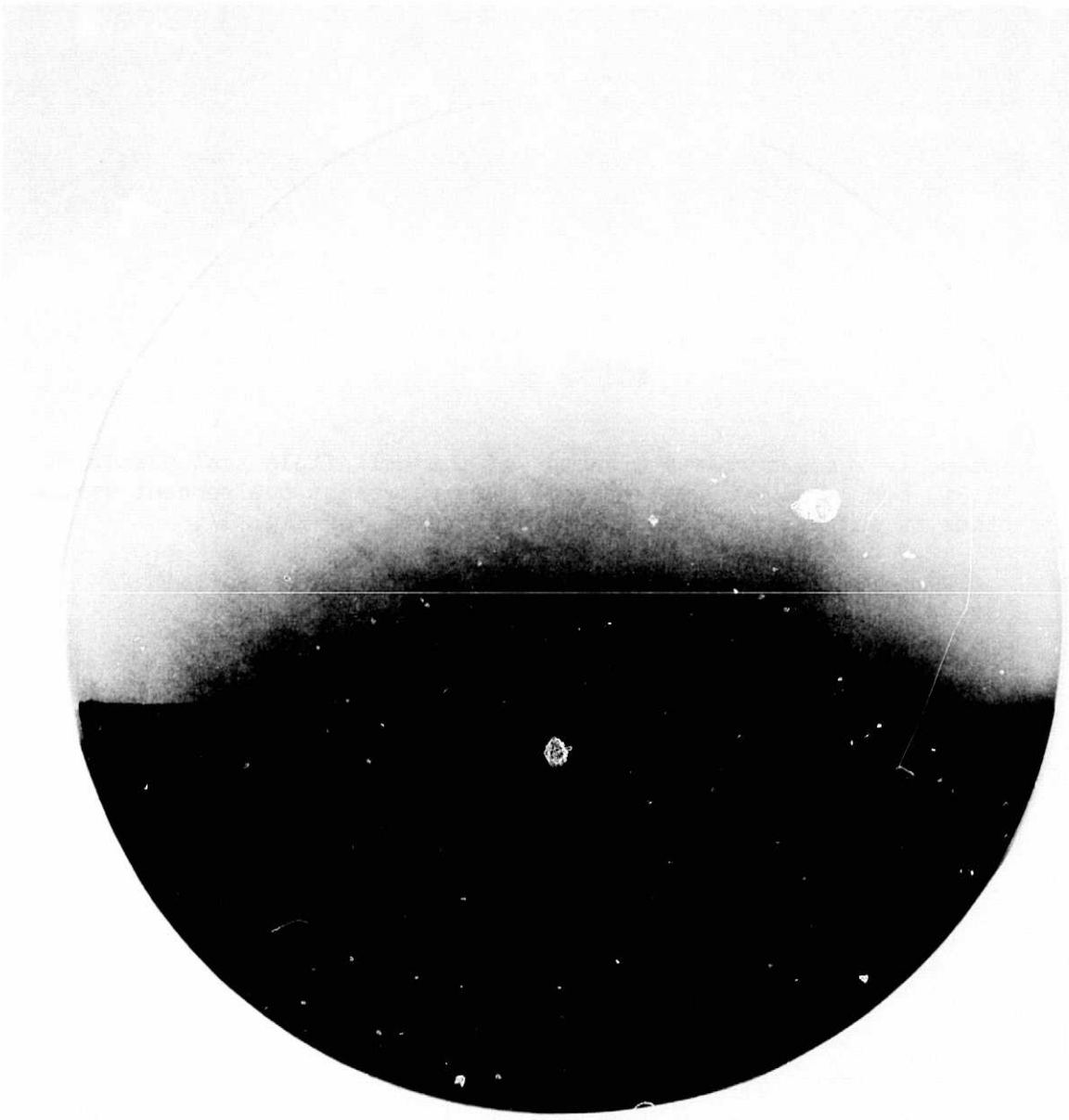

FIGURE 22

Intensity scans across a diameter of the half field test plates at 3500Å, 8000Å and 9019Å. Vertical bars represent one percent variations in intensity. Scanning parameters as for Fig. 17.

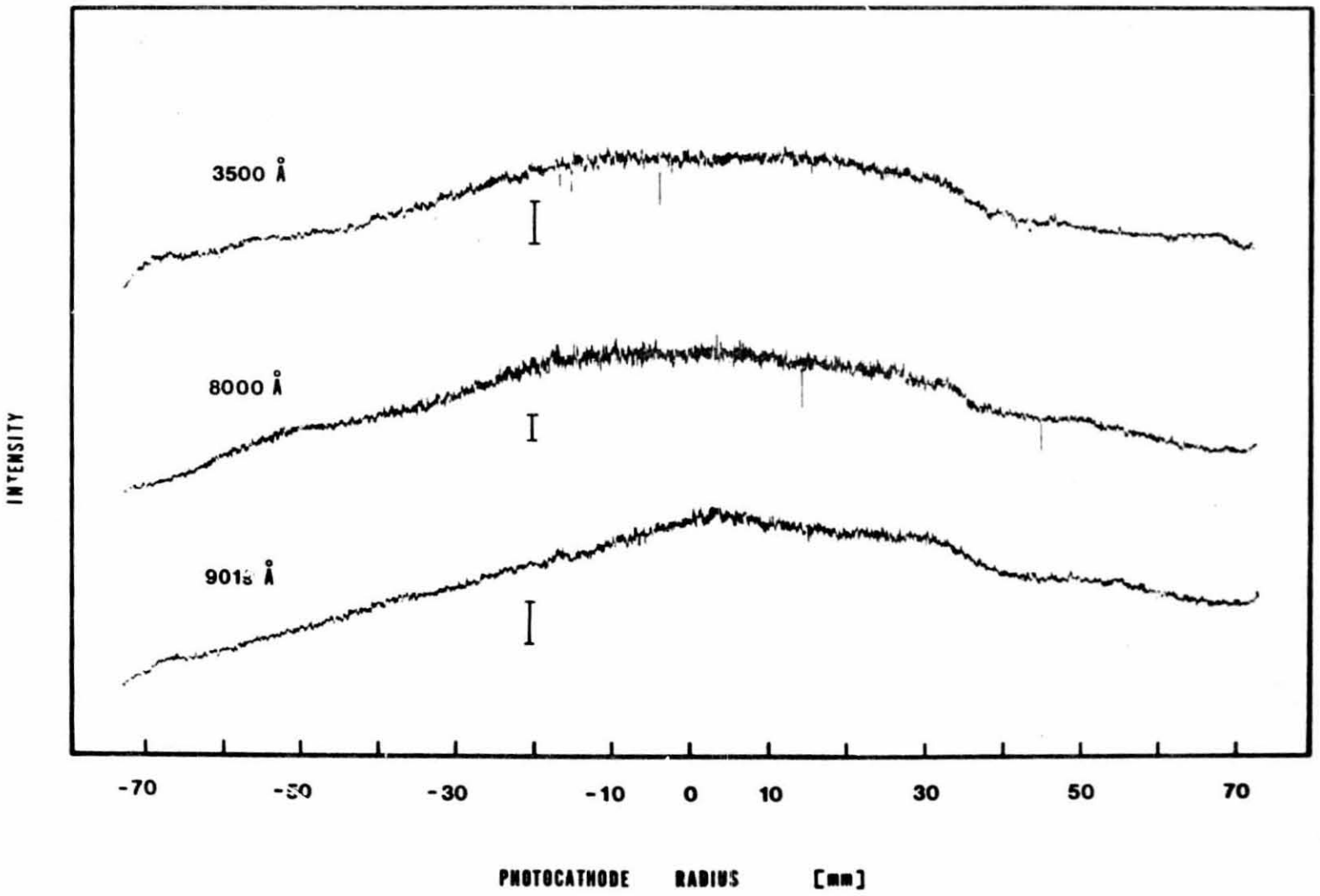
3500 Å
8000 Å
9018 Å
INTENSITY
-70
-50
-30
-10
0
10
30
50
70
PHOTOCATHODE RADIUS [mm]

In practice we rarely use exposures as long as one hour and have never exceeded this exposure time.

G. Detective Quantum Efficiency

Detective quantum efficiency (DQE) is defined as

$$DQE = \frac{(S/N)^2_{out}}{(S/N)^2_{in}}$$

where S/N represent the signal to noise ratios, both input and output. DQE is a significant measure of the performance of a detector.

A detailed discussion of the techniques employed in determining DQE can be found in Smith (1972). We have used the gradient method in arriving at a measure of the DQE.

The image tube was exposed to a DQE sensitometer image (experimental apparatus shown in Fig. 23) using a set of attenuators in order to achieve a wide range of image densities. Each image is composed of a series of spots of known intensity which were densitometered in order to construct an H-D curve. In addition 14 large spots ($\sim 1 cm^2$) were exposed at a large range of exposures. All images were recorded on IIaD emulsions from the same batch and processed similarly.

Each of the 14 spots were raster scanned on a PDS microdensitometer using a 40μ square aperture; the mean density and standard deviation for each were then computed.

DQE for each density spot was then computed using the relationship

$$DQE = \frac{g^2 \bar{n} t}{\sigma_D^2 A}$$

where g is the slope of the H-D curve at the relevant density, $\bar{n}$ is the average irradience incident on the detector, t is the exposure time, σ_D

FIGURE 23

Optical bench set-up for DQE tests; 140mm image tube on the left and DQE sensitometer on the right.

is the standard deviation per measurement of density and A is the area of the scanning aperture.

DQE versus density for IIaD emulsion and 4250Å radiation is shown in Fig. 24. The image tube operating parameters are the same as discussed earlier in this report.

Both Smith (1972) and Cromwell and Dyvig (1973) present detailed discussions of the interpretation of DQE.

H. Tube Stability

The stability of the tube over short term and long term periods is extremely difficult to evaluate and unfortunately we have no precedent for this type of detector,

Short term stability problems of varying degrees of severity have been encountered in other types of tubes. In general we have not attempted to record data with this tube without about a one hour "warm up" period. However, a series of resolution tests were run within only a few minutes of voltage turn on and the results were completely compatable with those obtained with longer warm up periods. In particular there has been no evidence of gross field distortions which have been encountered by other researchers (Gull 1976).

Long term effects have not been systematically studied, in part because the tube has been in operation only a relatively short period of time. We can say qualitatively that the tube is still operated at the same voltage and current settings that were used a year ago with no apparent change in results. A more quantitative evaluation will require further monitoring as these tubes continue to be used in the future.

FIGURE 24

DQE(%) vs. density for the 140mm image tube plus IIaD plates at 4250Å.

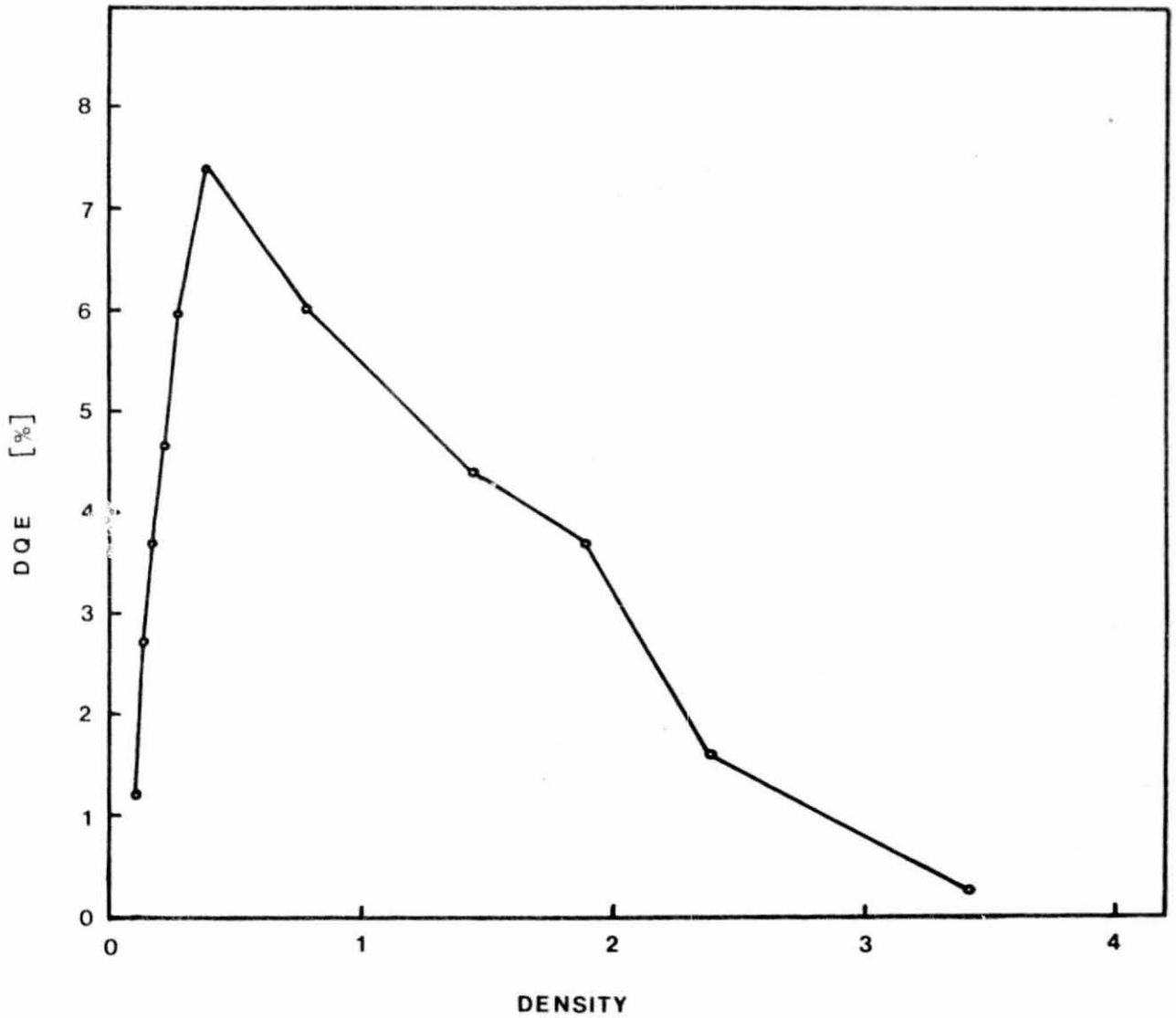
8
7
6
5
4
3
2
1
0
DQE [%]
0
1
2
3
4
DENSITY

V. ASTRONOMICAL USE OF THE LARGE FORMAT IMAGE TUBE

The 140mm image tube has been used for a variety of projects at the Cassegrain focus of the Steward Observatory 90" reflector. On the basis of this experience we can suggest a few areas in which the tube has had particularly successful applications.

1) Direct photography: Direct photography with a wide range of filters has been used for several programs. These programs include surface photometry of galaxies, morphological studies of BL Lac objects and study of radio source pairs. Plate scale at the 90" telescope is about 10"/mm and system resolution is about 30 μ. Limiting magnitudes on a IIaD plate with an RG10 filter and a 10^m exposure are typically about 21.0^m. Deeper plates of clusters of galaxies have been obtained with baked IIIaJ plates.

2) Polarization: Several programs have used the image tube in conjunction with a polaroid or calcite plate in order to obtain photographs of galaxies or BL Lac objects in polarized light. This type of program has been particularly successful in the discovery of new BL Lac objects.

3) Multi-color photography: We have experimented with obtaining multi-color (U,B,V and night sky red) photographs of star fields by translating the telescope after each exposure and by calibrating exposure times so that an A0 star appears neutral (all images the same size on the plates). This technique is useful for differentiating between objects which may appear similar on the Palomar plates (e.g. white dwarfs and QSO's).

4) Transmission grating spectroscopy: all field, low dispersion spectroscopy is possible by the introduction of a transmission grating in the optical path. This technique has been demonstrated feasible but has not been extensively used at Steward Observatory.

5) Narrow band photography: There are applications of narrow band photography with the image tube system which have been used at Steward Observatory. The high gain of the tube makes this sort of work feasible on reasonable time scales (photographic speed gain ~40).

6) Wide field survey work: We are in the process of adapting the 140mm image tube camera for wide field near infrared survey work. Because of the red extended response of the tube it is possible to obtain near infrared photographs to a limit of about 18^m in the 0.8 to 0.9μ region with exposure times of about 15^m. This approach permits study of large regions of the sky which are otherwise obscured by hydrogen emission.

An example of a photograph obtained with the 140mm image tube at the Cassegrain focus of the 90" telescope appears in Fig. 25. Additional discussions of specific applications of this tube may be found in the following papers:

Butcher, H., Oemler, A., Tapia, S. and Tarenghi, M. 1976, Ap. J. (in press).

Craine, Eric R., Tapia, S. and Tarenghi, M. 1975, Nature, 258, 56.

Craine, Eric R. and Warner, John W. 1976, Ap. J., 206, 359.

Ney, E. P. 1975, Sky and Tel., 45, No. 1. 21.

FIGURE 25

NGC 7331: 140mm image tube at the Cassegrain focus of the Steward 90" telescope; 10min. exposure on 103aD emulsion with NS red filter.

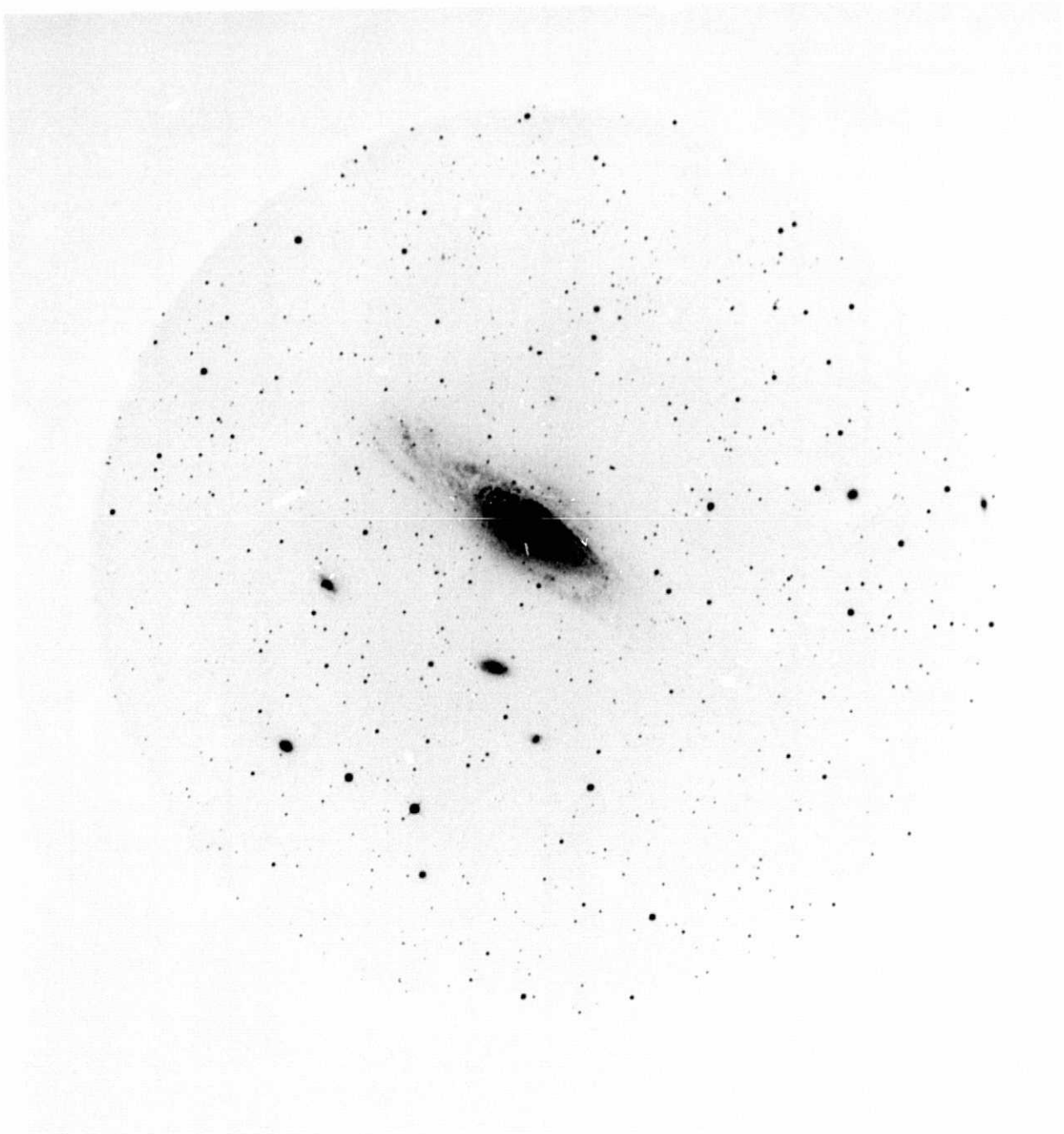

BIBLIOGRAPHY

Cromwell, R.H. and Dyvig, R.R. "Laboratory Evaluation of Eleven Image Intensifiers", Opt. Sci. Cen. Tech. Rep. 81, University of Arizona, August 1973.

Eastman Kodak "Kodak Plates and Films for Science and Industry", Kodak Publ. No. P-9, Eastman Kodak Co., Rochester, N.Y., 1967.

Gull, T.R. private communication, 1976.

Smith, Gregory H. "Evaluation of Image Intensifier Tubes Using Detective Quantum Efficiency", Opt. Sci. Cen. Tech. Rep. 76, University of Arizona, July 1972.